View metadata, citation and similar papers at core.ac.uk

brought to you by CORE

provided by Elsevier - Publisher Connector

Biochimica et Biophysica Acta 1793 (2009) 1676–1690

Contents lists available at ScienceDirect

Biochimica et Biophysica Acta

journal homepage: www.elsevier.com/locate/bbamcr

Identification of DH IC-2 as a HIF-1 independent protein involved in the adaptive response to hypoxia in tumor cells: A putative role in metastasis

Sebastien Pyr dit Ruys, Edouard Delaive, Catherine Demazy, Marc Dieu, Martine Raes, Carine Michiels *

URBC, University of Namur-FUNDP, rue de Bruxelles 61, B-5000 Namur, Belgium

ARTICLE INFO

Article history:
Received 24 March 2009
Received in revised form 27 August 2009
Accepted 1 September 2009
Available online 8 September 2009

Keywords:
Hypoxia
Cancer
Dynein
Metastasis
HIF-1 independent
Proteomics

ABSTRACT

The master regulator of the adaptive response to hypoxia is HIF-1. However, while some data show that HIF-1 can control more than 80% of the genes induced under hypoxia, other experiments clearly demonstrate that a part of the hypoxic response is independent of HIF-1. The goal of this study was to identify some of these HIF-1 independent factors and to investigate their functional role in the adaptation of tumor cells to hypoxia. We show that the cytoplasmic dynein intermediate chain 2 (DH IC-2), a component of an intracellular ATPase minus-end directed tubulin-based motile complex, was stabilized and post-translationally modified under hypoxia in a HIF-1 independent way. We identified this modification as a phosphorylation by protein kinase C, which is inhibited under hypoxia. In parallel, the migration of HepG2 cells was enhanced under hypoxia. Cell migration was also increased, to the same extent, by the invalidation of DH IC-2 using siRNA. Taken together, these results suggest that under hypoxia, a specific modification of DH IC-2 may modulate its activity, and in turn promote cell migration. These results are important to better understand cancer development since they highlight a HIF-1 independent mechanism, which may be involved in metastasis.

© 2009 Elsevier B.V. All rights reserved.

1. Introduction

Oxidoreduction mechanisms are the most predominant way to provide energy supply to mammalian cells, which in turn allow cell survival and growth [1]. Hypoxia is characterized by a decrease in oxygen availability, and cells have to adapt in order to survive to this condition. The master regulator of this adaptive response to hypoxia is HIF-1 [2,3]. This transcription factor is a member of the bHLH-PAS family and is composed of two subunits: HIF-1α and ARNT (aryl hydrocarbon receptor nuclear translocator) [4]. HIF-1α is the regulatory subunit of HIF-1 and is subjected to proteosomal degradation under normoxic conditions [5]. Under hypoxia, HIF-1α is stabilized and translocates into the nucleus where it associates with its constitutively expressed partner ARNT, which is also known to be involved in xenobiotic detoxification pathway [6]. HIF-1 can transactivate a variety of genes involved in multiple pathways such as glycolysis (enolase, aldolase, glucose transporter 1/3) [3], angiogenesis [VEGF (vascular endothelial growth factor), VEGF-receptor 1] [7], cell survival (Mcl-1) [8] and invasion (stromal cell derived factor 1-alpha, matrix metalloproteinase 1) [9].

Within a tumor, hypoxia can occur at different states of its development [10,11]. For example, when a tumor is growing, the cells close to the blood vessels are well oxygenated, but when the tumor mass expends, some cells are rejected to its periphery and they become being too far to receive oxygen by diffusion from adjacent capillaries [12]. Tumor cells also become hypoxic in case of blood flow arrest caused by any vascular problem like blood clot, by shunt or simply by the irregular blood flow observed in the immature tumor vascular system [13].

Hypoxic conditions are important in cancer resistance to therapeutic treatments and are often associated with a poor patient prognosis [14]. This is due to a reduced accessibility of drugs to the hypoxic regions [15], to multi-drug resistant channel overexpression in hypoxic tumor cells [16] and to protection from cell death by blockade of some apoptotic pathways [17].

Consequently, several strategies are now developed aimed to invalidate the adaptive response of tumor cells to hypoxia [18]. Most of these approaches target the HIF-1 pathway or the VEGF receptor, and promising results have already been obtained [19]. However, while some data showed that HIF-1 could control until 80% of the genes induced under hypoxia [2], other experiments clearly demonstrated that a part of the hypoxic response is independent of HIF-1 [20–23]. In that way, and as tumor cells are well known to raise a high plasticity and to be able to escape from numerous regulatory mechanisms, it is important to better understand the HIF-1 independent actors of the adaptive response to hypoxia.

The goal of this study was to identify some of these HIF-1 independent factors and to investigate their functional role in the adaptation of tumor cells to hypoxia. For this purpose, we used the

* Corresponding author. URBC, rue de Bruxelles 61, B-5000 Namur, Belgium. Tel.: +32 81 724131; fax: +32 81 724135.
E-mail address: carine.michiels@fundp.ac.be (C. Michiels).

0167-4889/$ – see front matter © 2009 Elsevier B.V. All rights reserved.
doi:10.1016/j.bbamcr.2009.09.003

human hepatic cell line HepG2, a well-established hypoxia tumor cell model [8], exposed to the chemical compound $CoCl_2$, a well-known inducer of HIF-1 [24] or to true hypoxia.

In this report, we show that the cytoplasmic dynein intermediate chain 2 (DH IC-2), a component of an intracellular ATPase minus-end directed tubulin-based motile complex [25], was stabilized and post-translationally modified under hypoxia, in a HIF-1 independent way. DH IC-2 was phosphorylated by protein kinase C (PKC) under normoxia and was found to be de-phosphorylated under hypoxia. Dynein is a large multi-subunit protein principally composed of four components: the heavy chain (530 kDa), the intermediate chain (75 kDa), the light intermediate chain (30–50 kDa) and the light chain (10–14 kDa) [26]. Dyneins are clustered in two groups: cytoplasmic and axonemal [27]. Cytoplasmic dyneins are involved in intracellular transport, mitosis, cell polarization and directed cell movement [28]. Axonemal dyneins are responsible for ciliary and flagellar beating [29]. We also showed that the migration of HepG2 cells was enhanced under hypoxia and, to the same extent, by the invalidation of DH IC-2 using siRNA. These results suggest that under hypoxia, a specific modification of DH IC-2 may modulate its activity, and in turn promote cell migration.

2. Materials and methods

2.1. Cell culture and stimulation

Murine hepatoma HepaC4 cells (kindly donated by Prof. Hankinson, UCLA) were cultured in Dulbecco's modified Eagle's medium high glucose-4000 mg/l (DHG) (Gibco, Paisley, UK) supplemented with L-glutamine (Sigma Aldrich, St. Louis, MO) containing 10% fetal calf serum (Gibco, Paisley, UK) at 37 °C and 5% CO_2. Cells were plated at 80% 1 day before the incubation under hypoxic or normoxic conditions.

Human hepatoma HepG2 cells (ATCC) were grown in Dulbecco's modified Eagle's medium low glucose-1000 mg/l (DMEM) (Gibco, Paisley, UK) supplemented with L-glutamine (Sigma, St. Louis, MO) containing 10% fetal calf serum (Gibco, Paisley, UK) at 37 °C and 5% CO_2. Cells were plated at 8×10^4 cells/$_{cm2}$ 1 day before the incubation under hypoxic or normoxic conditions.

Hypoxia incubations were performed in serum-free CO_2-independent medium (Gibco, Paisley, UK) supplemented with 10 mM L-glutamine (Sigma Aldrich, St. Louis, MO) under 99% N_2 and 1% O_2. Control normoxic cells were maintained under normal atmosphere (20% O_2). The oxygen concentration in the medium obtained in our experimental conditions is 10 mmHg.

Cycloheximide at 20 μM (CHX) (Sigma Aldrich, St. Louis, MO), MG132 at 20 μM (Biomol/Tebu-Bio Boechout, Belgium), calphostin C at 2 μM (El-198, Biomol/Tebu-Bio Boechout, Belgium), SB203580 at 20 μM (Alexis, Hausen, Switzerland), DRB at 100 μM (5,6-dichloro-1-β-D-ribofuranosyl-benzimidazole, Biomol/Tebu-Bio Boechout, Belgium), PMA at 0.3 μM (phorbol-12-myristat-13-acetate, Sigma Aldrich, St. Louis, MO) and $CoCl_2$ at 150 μM (Sigma Aldrich, St. Louis, MO) incubations were performed in serum-free CO_2-independent medium (Gibco, Paisley, UK) supplemented with 10 mM L-glutamine (Sigma Aldrich, St. Louis, MO). All supplemented media were filtered on 0.22 μm porous membrane.

2.2. 2D DIGE analyses

2.2.1. Sample preparation

After elimination of the medium, cells were collected in 1 ml of pre-cooled PBS, transferred into microtubes and centrifuged 4 min at 1000 rpm at 4 °C. The pellets were lysed with the DIGE Labeling (DLA) buffer (CHAPS 4%, urea 7 M, thiourea 2 M, Tris 30 mM, pH 8.5) and clarified by centrifugation at 13,000 rpm for 5 min at 4 °C.

2.2.2. Protein labeling

Protein concentrations were determined in triplicates by the Bradford method (Bio-Rad, München, Germany) and extracts were diluted to reach a final concentration of 5–10 μg/μl. The pH of the samples was adjusted to 8.5. Each sample (25 μg) was minimally labeled with the CyDyes DIGE (Amersham GE Healthcare, Uppsala, Sweden) during 30 min in the dark (200 pmol of amine-reactive cyanine dyes, Cy3 or Cy5) at 4 °C following the manufacturer's instructions. An internal standard, obtained after pooling an equal amount of the six different samples, was labeled with Cy2. Labeling was stopped by incubating the mixture 10 min with 1 μl of 10 mM lysine (Sigma Aldrich, St. Louis, MO). Each gel was then loaded with 25 μg of mixed labeled samples (normoxia and normoxia + $CoCl_2$, or normoxia and hypoxia) and 25 μg of the internal standard. The different mixes of proteins were diluted twice (CHAPS 4%, urea 7 M, thiourea 2 M, Tris 30 mM, DTT 30 mM, IPG buffer 4–7 (v/v) 1%) (Amersham GE Healthcare, Uppsala, Sweden) and reduced 20 min in the dark at room temperature before clarification by centrifugation at 13,000 rpm during 10 min.

2.2.3. Two-dimensional differential in-gel electrophoresis

The first dimension was performed with Immobiline DryStrips (IPG strip continuous pH 4–7 gradient 24 cm; Amersham GE Healthcare, Uppsala, Sweden). IPG strips were rehydrated in an Immobiline DryStrip reswelling tray (Amersham GE Healthcare, Uppsala, Sweden) for 24 h at RT with 450 μl of rehydration buffer (CHAPS 4%, urea 7 M, thiourea 2 M, Tris 30 mM, DTT 30 mM, IPG buffer 4–7 (v/v) 0.5%) and covered with 2.5 ml DryStrip oil. Samples were loaded in a cupule at the more acidic part of the IPG strips. Isoelectric focusing (IEF) was run on an IPGphor isoelectric focusing system (Amersham GE Healthcare, Uppsala, Sweden) with the following parameters: 300 V for 3 h, gradient step of 1000 V for 8 h, gradient step of 8000 V for 3 h and 8000 V for 65,000 V/h at 20 °C with a maximum current setting of 50 μA/strip. IPG strips were then washed with distillated water, and incubated subsequently for 15 min with an equilibration buffer [Tris–HCl 50 mM (pH 8.8), urea 6 M, glycerol (v/v) 30%, SDS (w/v) 2%] supplemented with DTT 10 mg/ml or iodoacetamide 25 mg/ml, respectively. The IPG strips were then washed with running buffer [Tris–HCl 50 mM (pH 8.5), glycine 384 mM, SDS 0.2%] twice concentrated and sealed with agarose 0.5% (containing bromophenol blue) on the top of a 10% SDS–PAGE pre-poured between low fluorescent glass plates using an Ettan-DALT caster (Amersham GE Healthcare, Uppsala, Sweden). Twice concentrated buffer and normal running buffer were added at the top and the bottom of the gels, respectively. Electrophoresis was performed overnight (16 h) at 14 °C with 1 W/gel in the EttanDalt II system (Amersham GE Healthcare, Uppsala, Sweden). The three gels from a same experiment were run at the same time.

2.2.4. Image acquisition and statistical analysis

In order to observe cyanin-labeled proteins, gels were scanned in fluorescence with Typhoon 9400 imager (Amersham GE Healthcare, Uppsala, Sweden) at a resolution of 100 μm. Cy2 images were obtained from a 488 nm excitation laser coupled to a 520 nm emission filter. Cy3 images were obtained from a 532 nm excitation laser coupled to a 580 nm emission filter. Cy5 images were obtained from a 633 nm excitation laser coupled to a 670 nm emission filter. A total of nine gel images was generated for each comparative experiment and analyzed using DeCyder Differential Analysis Software v6.0 (Amersham GE Healthcare, Uppsala, Sweden) for spot detection, matching, quantitation and statistical analysis. First, a differential in-gel analysis (DIA) was applied on each gel to eliminate gel-to-gel variance by matching and normalizing every spot gel with the corresponding internal standard. Second, a biological variation analysis (BVA) software, using student's t test ($p<0.05$), was run to detect statistical

differential protein expression between the control and treated groups. Depending on the experiment, spots of interest were defined as spots with at least 1.3- or 1.5-fold change in abundance after normalization.

2.2.5. Sample recovering

A preparative 2D gel was performed with 300 μg of unlabeled proteins obtained by pooling the same amount of proteins from the six samples used for the analytical gels. The protocol remained unchanged as for analytical gels except that the sample was loaded in two times for the first dimension in order to decrease protein precipitation; for the second dimension, one of the low fluorescent glass plates was pre-treated with bind-silane (Amersham GE Healthcare, Uppsala, Sweden). At the end, the plate without bind-silane was removed and the gel was incubated in a fixating solution (ethanol 30%, acetic acid 10%) for 5 h. Gels were then washed three times for 30 min with distilled water before overnight protein staining with 1 l of ethanol 20% supplemented with 7 μl of 20 mM Ruthenium II solution [Ruthenium II tris (bathophenantroline disulfonate)]. Gels were then washed twice with distilled water (Milli-Q system, Millipore, Bedford, MA) for 10 min. Gels were scanned with Typhoon 9400 imager (Amersham GE Healthcare, Uppsala, Sweden) using a 532 nm excitation laser coupled to a 610 nm emission filter. After matching the preparative gel picture to the master analytical gel image, spots of interest were localized on the preparative gel and picked with an automated Ettan Spot Picker (Amersham GE Healthcare, Uppsala, Sweden) following the manufacturer's instructions. Spots were transferred in a 96-well plates and kept frozen at −20 °C until protein digestion.

2.2.6. Protein extraction and digestion

Gel fragments were washed twice with distilled water (Milli-Q system, Millipore, Bedford, MA) and once with acetonitril (ACN) 100% at 900 rpm and 21 °C for 10 min. Pellets were then dried at 56 °C, reduced with DTT 10 mM (Sigma Aldrich, St. Louis, MO) in NH_4HCO_3 100 mM during 45 min at 900 rpm and 56 °C, before alkylation through incubation in iodoacetamide 55 mM in NH_4HCO_3 100 mM during 30 min in the dark. Gel fragments were washed with distilled water (Milli-Q system, Millipore, Bedford, MA), twice with ACN 100% for 5 min at 900 rpm, once with NH_4HCO_3 100 mM at 900 rpm for 5 min and once with ACN 100% at 900 rpm for 10 min. Pellets were dried at 37 °C during 20 min. Proteins were first digested on ice with trypsin 12.5 ng/μl (Promega, Madison) in 50 mM NH_4CO_3 for 45 min, and then overnight at 37 °C. Peptides were extracted with 10 μl acid formic 5% and the collected supernatants were kept frozen at – 20 °C until mass spectrometry analysis.

2.2.7. Protein identification

Digested peptides were first separated on a nano C18 column (Atlatis, 75 μM, 150 mm, 3 μm NanoEase column; Waters, Milford) and then identified by Nano-LC-QTOF-MSMS. The mass spectrum of peptide fragments was obtained through the use of a CapLC in tandem with a Q-time-of-flight 2 (Q-TOF2) (Waters, Milford) coupled to the MassLynx 4.0 software (Waters, Milford).

Some proteins were also identified on the basis of their "peptide mass fingerprint" obtained with a matrix-assisted laser desorption/ionization MX (Maldi) (Waters, Milford). Peptide mass maps were acquired in the reflectron mode with delayed extraction. Mass spectra were internally calibrated with trypsin autolysis peaks.

Full-length proteins were identified with Mascot software (version 2.0) (Matrix Sciences, London, UK) by sequence homology research against human or murine protein databases.

2.2.8. Western blot

After elimination of the medium, cells were collected in 1 ml of pre-cooled PBS and transferred into microtubes. Microtubes were centrifuged 4 min at 1000 rpm at 4 °C. Supernatants were removed and pellets were lysed with the extraction buffer [Tris 80 mM, pH 7.5 (Merck, Darmstadt, Germany), KCl 300 mM (Merck, Darmstadt, Germany), EDTA 2 mM (Merck, Darmstadt, Germany), Triton X-100 1% (v/v) (Sigma, St. Louis, MO), containing a protease inhibitor mixture (≪Complete≫ from Roche Molecular Biochemicals, 1 tablet in 2 ml H_2O, added at a 1:25 dilution) and phosphatase inhibitors ($NaVO_3$ 25 mM, PNPP 250 mM, β-glycerophosphate 250 mM and NaF 125 mM, at a 1:25 dilution)]. Microtubes were then centrifuged 4 min at 13,000 rpm at 4 °C. Supernatants were collected and stored at −80 °C. Protein concentrations were determined according to the Bradford method (Bio-Rad, München, Germany). Equal amounts of protein (20–40 μg) were then separated by SDS–PAGE on 10% acrylamide gel and transferred to a polyvinyldiene difluoride membrane (Amersham Biosciences, Uppsala, Sweden). Membranes were blocked with Tris buffer saline supplemented with 0.1% (v/v) Tween and 2% (w/v) dried milk (ECL detection kit, Amersham GE Healthcare, Uppsala, Sweden), and probed with the following antibodies: anti-HIF-1α antibodies (BD Transduction Laboratories; diluted 1:2000), secondary antibody anti-mouse horseradish peroxidase-conjugated (Amersham GE Healthcare, Uppsala, Sweden; diluted 1:300,000), anti-α-tubulin antibodies (Sigma, St. Louis, MO; diluted 1:50,000), secondary antibody anti-mouse horseradish peroxidase-conjugated (Amersham GE Healthcare, Uppsala, Sweden; diluted 1:300,000), anti-DH IC-2 intermediate chain antibodies (Abcam #ab6304, clone 70.1; diluted 1:50,000), secondary antibody anti-mouse horseradish peroxidase-conjugated (Amersham GE Healthcare, Uppsala, Sweden; diluted 1:300,000), anti-p53 antibodies (Upstate; diluted 1:5000), and secondary antibody anti-mouse horseradish peroxidase-conjugated (Amersham GE Healthcare, Uppsala, Sweden; diluted 1:300,000). Proteins were detected by chemoluminescence (ECL detection kit, Amersham GE Healthcare, Uppsala, Sweden) using a Fujifilm FPM-100A (Fujifilm, Düsseldorf, Germany). Films were scanned with the Image Master Labscan V2003.01 Software (Amersham GE Healthcare, Uppsala, Sweden) and semi-quantitated with the ImageQuant TotalLab V2,3.03 software (Amersham GE Healthcare, Uppsala, Sweden).

2.2.9. 2D-blot

Cells were collected and lysed and 100 μg of each sample were prepared as for 2D preparative gels. First dimension was performed with Immobiline DryStrips (IPG strip continuous pH 4–7 gradient, 18 cm; Amersham GE Healthcare, Uppsala, Sweden) pre-rehydrated during 24 h at RT with 350 μl of rehydration buffer (CHAPS 4%, urea 7 M, thiourea 2 M, Tris 30 mM, DTT 30 mM, IPG buffer 4–7 (v/v) 0.5%). Samples were loaded as for 2D gels, and ran with the following parameters: 300 V for 3 h, gradient step of 1000 V for 8 h, gradient step of 8000 V for 3 h and 8000 V for 25,000 V/h at 20 °C with a maximum current setting of 50 μA/strip [IPGphor isoelectric focusing system, Amersham GE Healthcare, Uppsala, Sweden]. IPG strips were then washed, equilibrated and sealed with agarose 0.5% (containing bromophenol blue) on the top of a 10% SDS–PAGE as for 2D gels. After protein separation, samples were transferred to a polyvinyldiene difluoride membrane (Amersham Biosciences, Uppsala, Sweden), blocked with phosphate saline buffer supplemented with 0.1% (v/v) Tween and 2% (w/v) dried milk (ECL detection kit, Amersham GE Healthcare, Uppsala, Sweden) and probed as described for Western blot. The three gels of a same experiment were run at the same time.

2.2.10. Immunoprecipitation

HepG2 cells were seeded at 80,000/cm2 in DMEM + 10% FBS and grown for 24 h before starting the experiments. After the incubation, cells were lysed in 1 ml IP lysis buffer [25 mM Tris, pH 7.8, 100 mM NaCl, 1 mM EDTA, 10% glycerol (Merck, Darmstadt, Germany), 0.2% NP-40 (Sigma, St. Louis, MO), 1 mM DTT (Sigma, St. Louis, MO), 1 mM

PMSF (Sigma, St. Louis, MO), 5 mM NaF (Merck, Darmstadt, Germany), 1 mM $NaMoO_4$ (Sigma, St. Louis, MO) and 60 μM MG132 (Biomol/Tebu-Bio Boechout, Belgium)]. An aliquot of 50 μl was kept for assessing the protein level of DH IC-2 in the cell extracts. Lysates were incubated 2 h at 4 °C with 2.5 μg of anti-DH IC-2 IgG, then 2 h at 4 °C with 50 μl proteinA/G coated beads (BD bioscience). The beads were washed three times with 800 μl of the IP lysis buffer, after which DH IC-2 was recovered by incubating the beads in Laemmli buffer for 10 min at 100 °C. Samples were resolved on 10% SDS–PAGE and transferred on polyvinyldiene difluoride membrane. Proteins were detected with anti-DH IC-2 or pan-serine/threonine specific IgG (#44-006, Upstate, Lake Placid).

2.2.11. PKC kinase activity assay

HepG2 cells were seeded at 80,000/cm2 in DMEM + 10% FBS and grown for 24 h before starting the experiments. After the incubation, the medium was removed and replaced with 1 ml of fresh lysis buffer [20 mM MOPS (Merck, Darmstadt, Germany), 50 mM α-glycerophosphate (Prolabo, Pennsylvania), 50 mM sodium fluoride (Merck, Darmstadt, Germany), 1 mM sodium vanadate (Sigma), 5 mM EGTA (Sigma, St. Louis, MO), 2 mM EDTA (Merck, Darmstadt, Germany), 1% (v/v) NP40 (Sigma, St. Louis, MO), 1 mM dithiothreitol (DTT) (Sigma, St. Louis, MO), 1 mM benzamidine (Sigma, St. Louis, MO), 1 mM phenylmethanesulphonylfluoride (PMSF) (Sigma, St. Louis, MO) and protease inhibitors 4% (v/v) (Complete®; Roche)] and was added per T25 flask and the flasks were put on ice. After 10-min incubation period, cells were scraped using a cell scraper and cell lysates were collected in a pre-chilled 1.5 ml microtube kept on ice. Microtubes were centrifuged at 13,000 × *g* for 15 min at 4 °C. Clear supernatant was transferred to a pre-chilled 1.5 ml microtube and protein concentration was determined using Bradford method. The assay was performed immediately after cell lysis using a PKC Kinase Activity Assay Kit (Non-Radioactive) (Assay Designs, Ann Arbor) with 20 μg of fresh lysate proteins for each condition.

2.2.12. Total RNA extraction and reverse transcription

After the incubation, the medium was removed and total RNA extraction was performed using RNAgents kit according to the manufacturer's instructions (RNAgents, Total RNA Isolation System, Promega, Madison). For each condition, 2 μg of total RNA were mixed with 2 μl oligo (dT) (500 ng/μl) (Gibco, Paisley, UK). The volume was then brought up to 9 μl with nuclease-free water (Promega, Madison). This mix was first incubated for 10 min at 70 °C and then on ice for 5 min. Reaction mix [9 μl; 4 μl Buffer RT 5X (Promega, Madison), 2 μl DTT 0.1 M (Promega, Madison), 1 μl RNAsin (40 U/μl) (Promega, Madison), 2 μl dNTP mix (Eurogentec, Seraing, Belgium)] was added and the samples were left for 5 min at room temperature. After addition of 1.5 μl SuperScriptRII (200 U/μl) (Invitrogen, Carlsbad), the samples were incubated for 90 min at 42 °C and then for 15 min at 70 °C. Finally, 1 μl of Ribonuclease H (2 U/μl) (Gibco, Paisley, UK) was incubated with the samples for 20 min at 37 °C before being stored at −20 °C. Sequences of the primers were determined using Primer Express 1.5 software (Applied Biosystems, Foster City): DH IC-2, 5′-AACACAAAATGCTCACAA-TCTGATTAG-3′ (forward) and 5′-TGCTATCCTGTGGATGGGAAA-3′ (reverse); aldolase, 5′-TGCGCAGGAGGAGTATGTCA-3′ (forward) and 5′-AGGCGTGGTTAGAGACGAAGAG-3′ (reverse); Rpl13, 5′-GCCTACAAGAAAGTTTGCCTATCTG-3′ (forward) and 5′-TGAGCTGTTTCTTCTTCCGGTAGT-3′ (reverse). cDNAs and primer concentrations were experimentally determined to allow PCRs to remain in the exponential zone of amplification, and the specificity of the PCR was checked by carrying out a dissociation curve with a gradient from 60 °C to 95 °C. cDNAs (5 μl) were added to SYBR Green Master Mix PCR [2.5 μl distilled water, 1.7 μl of reverse primer at 9 μM, 1.7 μl of forward primer at 9 μM, 12.5 μl of SYBR green] and PCRs were performed in 7900 HT Fast Real Time PCR System (Applied Biosystems, The Netherlands) using SDS 2.2.1 Software (Applied Biosystems, The Netherlands). Thermal cycling conditions were as follows: 2 min at 50 °C, 10 min at 95 °C, 40 cycles of 30 s at 95 °C, 1 min at 57 °C and 30 s at 72 °C. Rpl13 amplification was used as a standard to normalized differences between samples, and fold induction was estimated with the classical "$\Delta\Delta C_T$ method" [30]. PCR efficiency was higher than 90% for all genes.

2.2.13. Immunofluorescence

HepG2 cells were seeded at $25{,}000/_{cm2}$ in DMEM + 10% FBS and grown on glass cover slide for 24 h before starting the experiments. After the incubation, the medium was removed, and cells were fixed for 10 min with PBS containing 4% (w/v) paraformaldehyde (Merck, Darmstadt, Germany). Fixed cells were washed three times with PBS and permeabilized with PBS–Triton X-100 1% (w/v) (Sigma, St. Louis, MO) during 4 min. After three washing steps with PBS containing 2% (w/v) bovine serum albumin (BSA) (PAA Laboratories), cells were incubated during 2 h under wet atmosphere at room temperature with anti-DH IC-2 intermediate chain antibodies [Abcam #ab6304, clone 70.1; diluted 1:100 in PBS + 2% (w/v) BSA]. Cells were then washed three times with PBS + 2% (w/v) BSA, and the secondary antibodies conjugated to Alexa fluorochrome 488 [Molecular Probes; diluted 1:1000 in PBS + 2% (w/v) BSA] were added under wet atmosphere at room temperature for 1 h. The cells were then washed three times with PBS. Nuclei were labeled with Topro-3 [Molecular Probes; diluted 1:80 in PBS + RNase 2 mg/ml (ICN)] during 30 min. Finally, the cells were mounted in mowiol (Sigma, St. Louis, MO). Observations were performed with a confocal microscope using a constant photomultiplier (Leica, Groot Bijgaarden, Belgium).

2.2.14. Cell viability assay

HepG2 cells were seeded at a density of 12×10^3/cm2 in DMEM + 10% FBS and grown on 24 h before starting the experiments. After the incubation, cell viability was evaluated by 3-(4,5-dimethylthiazol-2-yl)-2,5-diphenyltetrazolium bromide reduction assay (MTT) (Sigma, St. Louis, MO) [31]. MTT solution was added volume-to-volume for 2 h at 37 °C under 5% CO_2, and then discarded before overnight incubation in lysis buffer [20% SDS (MP Biomedicals, Eschwege, Germany), 33.3% *N*,*N*-dimethyl-formamide (Merck, Darmstadt, Germany), pH 4.7] under shaking (100 rpm) at 37 °C in the dark. The OD values were recorded at 570 nm (plate reader Ultramark Microplate Imaging System, Bio-Rad, München, Germany).

2.2.15. Migration assay

HepG2 cells were plated (100,000/300 μl/well) in Boyden chambers, on the top of 8 μm pore polycarbonate membrane (Transwell, Costar, Corning, NY) in serum-free CO_2-independent medium (Gibco, Paisley, UK) supplemented with 10 mM L-glutamine (Sigma, St. Louis, MO). These chambers were maintained in 24-wells plates and 600 μl/well of CO_2-independent medium (Gibco, Paisley, UK) supplemented with 10 mM L-glutamine (Sigma, St. Louis, MO) and 10% FBS were placed at the bottom of wells as a chemotaxis inducer. After 24-h incubation, the cells having migrated on the other side of the porous membrane were stained with crystal violet [crystal violet 4.8 mM (Janssen, Geel, Belgium), ethanol 2%] as follows: Transwell inserts were first washed three times in PBS, fixed 45 s with methanol pre-cooled to −20 °C, washed three times with distilled water, incubated 45 s with crystal violet solution and washed three times with distilled water. The top of the porous membranes was then cleaned of cells twice with a cotton swab, cut with a scalpel blade and mounted with Glycergel (Dako, Denmark). Cover slides were maintained under weight overnight at room temperature to avoid air bubbles. Observations were performed with DIALUX 20EB photonic microscope (Leica, Groot Bijgaarden, Belgium) coupled

Table 1
List of HIF-1 independent hypoxia-responsive proteins identified by mass spectrometry in HepaC4 cells.

Master no.	Name	T-test	Av. Ratio	pI	Mw	Pept.	Protein ID	Comment
340	p137GPI	0.0039	−1.54	4.96	78120	5	Q61620	Regulates the transport and translation of mRNAs of proteins involved in synaptic plasticity in neurons and cell proliferation and migration in multiple cell types.
374	Alanyl tRNA synthetase	0.046	1.56	5.18	106647	6	Q8BXR0	Transfers alanyl on tRNA.
488	Cortactin	0.011	1.57	5.07	61222	14	Q60598	Involved in organization of cell structure. May contribute to cellular growth regulation and transformation.
488	Vasolin Containing Protein	0.011	1.57	4.95	89265	7	Q01853	Containing Protein Necessary for the fragmentation of Golgi stacks during mitosis, for the export of misfolded proteins from the ER to the cytoplasm. Regulates spindle disassembly.
516	Hypothetical Pyridoxal-Dependent Decarboxylase Family Protein	0.0086	2.54	5.22	78493	4	Q3TN13	Decarboxylase Family Protein Decarboxylase.
546	Ribonucleotide Reductase M1	0.0017	2.06	6.15	90093	7	Q91YM8	Provides the precursors necessary for DNA synthesis. Catalyzes the biosynthesis of deoxyribonucleotides from the corresponding ribonucleotides.
567	Ribonucleotide Reductase M1	0.00071	−2.11	6.15	90093	4	Q91YM8	Provides the precursors necessary for DNA synthesis. Catalyzes the biosynthesis of deoxyribonucleotides from the corresponding ribonucleotides.
600	Mitochondrial elongation factor G1	0.00085	2.1	6.35	83614	2	Q921D6	Promotes the GTP-dependent translocation of the nascent protein chain from the A-site to the P-site of the ribosome.
648	SUMO-activating enzyme subunit 2	0.048	−1.92	4.9	70524	14	Q3U9J5	Mediates ATP-dependent activation of SUMO proteins.
648	Dynein Cytoplasmic Intermediate Chain 2	0.048	−1.92	4.99	68351	9	Q3TGH7-3	Helps dynein bind to dynactin.
648	Cortactin	0.048	−1.92	5.07	61222	4	Q60598	Involved in organization of cell structure. May contribute to cellular growth regulation and transformation.
662	Dynein Cytoplasmic Intermediate Chain 2	0.0096	1.96	4.99	68351	11	Q3TGH7-3	Helps dynein bind to dynactin.
787	Lamin A/C	0.0009	1.89	6.54	74164	27	Q3TIH0	Component of the nuclear lamina.
793	TRIO and F-actin Binding protein	0.00036	−1.92	5.88	66938	14	Q99KW3	May regulate actin cytoskeletal organization, cell spreading and cell contraction by directly binding and stabilizing filamentous F-actin.
872	Phosphoglucomutase 2	0.01	−1.96	6.12	74164	8	Q9D0F9	Participates in both the breakdown and the synthesis of glucose.
887	Signal Transducing Adaptator Protein (SH3 domain and ITAM motif) 2	0.00051	2.28	4.76	57418	2	Q8C8Y4	Involved in intracellular signal transduction mediated by cytokines and growth factors. Plays a role in signaling leading to DNA synthesis and c-myc induction.
894	Lamin A/C	0.00059	−2.56	6.54	74164	15	Q3TIH0	Component of the nuclear lamina.
899	Lamin A/C	0.0016	−2.33	6.54	74164	23	Q3TIH0	Component of the nuclear lamina.
910	Lamin A/C	0.0068	1.5	6.54	74164	21	Q3TIH0	Component of the nuclear lamina.
920	Lamin A/C	0.0068	1.5	6.54	74164	32	Q3TIH0	Component of the nuclear lamina.
929	TCP-1 Epsilon	0.02	1.69	5.62	59585	13	Q3TIE0	Molecular chaperone. Known to play a role, in vitro, in the folding of actin and tubulin.
937	Dihydrolipoamide Dehydrogenase	0.028	1.74	7.81	54238	2	Q3UWP7	Component of the glycine cleavage system as well as of the alphaketoacid dehydrogenase complexes.
937	U3 snoRNP-associated protein	0.028	1.74	7.77	52074	1	Q8CFB7	Participates in the processing and modification of pre-ribosomal RNA.
1000	Vimentin	0.0029	1.78	4.86	53655	21	Q8CCH1	Class-III intermediate filaments.
1121	Aldehyde dehydrogenase 2	0.013	−1.67	6.01	48239	9	P47738	Converts retinaldehyde to retinoic acid.
1219	Cytokeratin 18	0.0044	1.68	5.04	47509	20	Q3TIX1	Plays a role in filament reorganization. Involved in the uptake of thrombin-antithrombin complexes by hepatic cells.
1254	Vimentin	0.018	1.68	4.86	53655	3	Q8CCH1	Class-III intermediate filaments.
1852	Stathmin	0.0007	1.56	5.87	17205	2	P54227	Prevents assembly and promotes disassembly of microtubules.
1856	Keratin	0.000016	3.46	7.74	61359	1	Q6IFZ6	Intermediate filament.

HepaC4 cells were incubated 16 h under hypoxia or normoxia. Hypoxia-responsive HIF-1 independent proteins were selected and then identified by mass spectrometry using a Nano-LC-QTOF-MSMS coupled to the MassLynx 4.0 software. Full-length proteins were identified with Mascot software (version 2.0) by sequence homology research against murine protein databases. T-test = Student's *t* test ($p<0.05$); Av. Ratio = biological variation in induction fold; pI = isoelectric point; Mw = molecular weight; Pept. = number of matching peptides.

with a DC100 camera (Leica, Groot Bijgaarden, Belgium), using DC100PPC software. Pictures were taken at the same swelling, contrast and luminosity.

2.2.16. siRNA transfection

In order to invalidate HIF-1α or DH IC-2 expression, si*GENOME* SMARTpool siRNA reagents M-0044018-02 and M-012574-00 were, respectively, ordered from Dharmacon (Erembodegem, Belgium). Non-targeting oligoribonucleotides D-00120-01-20 (Dharmacon, Erembodegem, Belgium) was used as negative control. One day before transfection, HepG2 cells were plated at 40×10^3/cm2 and grown in DMEM + 10% FBS. Cells were transfected according to the manufacturer's instructions (Dharmacon, Erembodegem, Belgium) for 24 h with siRNA at 50 nM in DMEM medium using Dharmafect 1 transfection reagent. Cells were seeded 24 h after transfection for the different assays.

2.2.17. In silico analysis tools

The in silico analysis tools are available online: http://www.cbs.dtu.dk/services/NetPhos/, http://www.ba.itb.cnr.it/BIG/UTRScan/, http://www.expasy.org/tools/ - ptm, http://www.matrixscience.com/.

Fig. 1. Representative proteomic maps (2D-gels). HepG2 cells were incubated 16 h under normoxia, normoxia + $CoCl_2$ 150 μM or hypoxia. Total cell extracts (75 μg) were isoelectrically focused and then separated as described in Materials and methods. The arrows with numbers represent spots with identified proteins which are listed in Table 2.

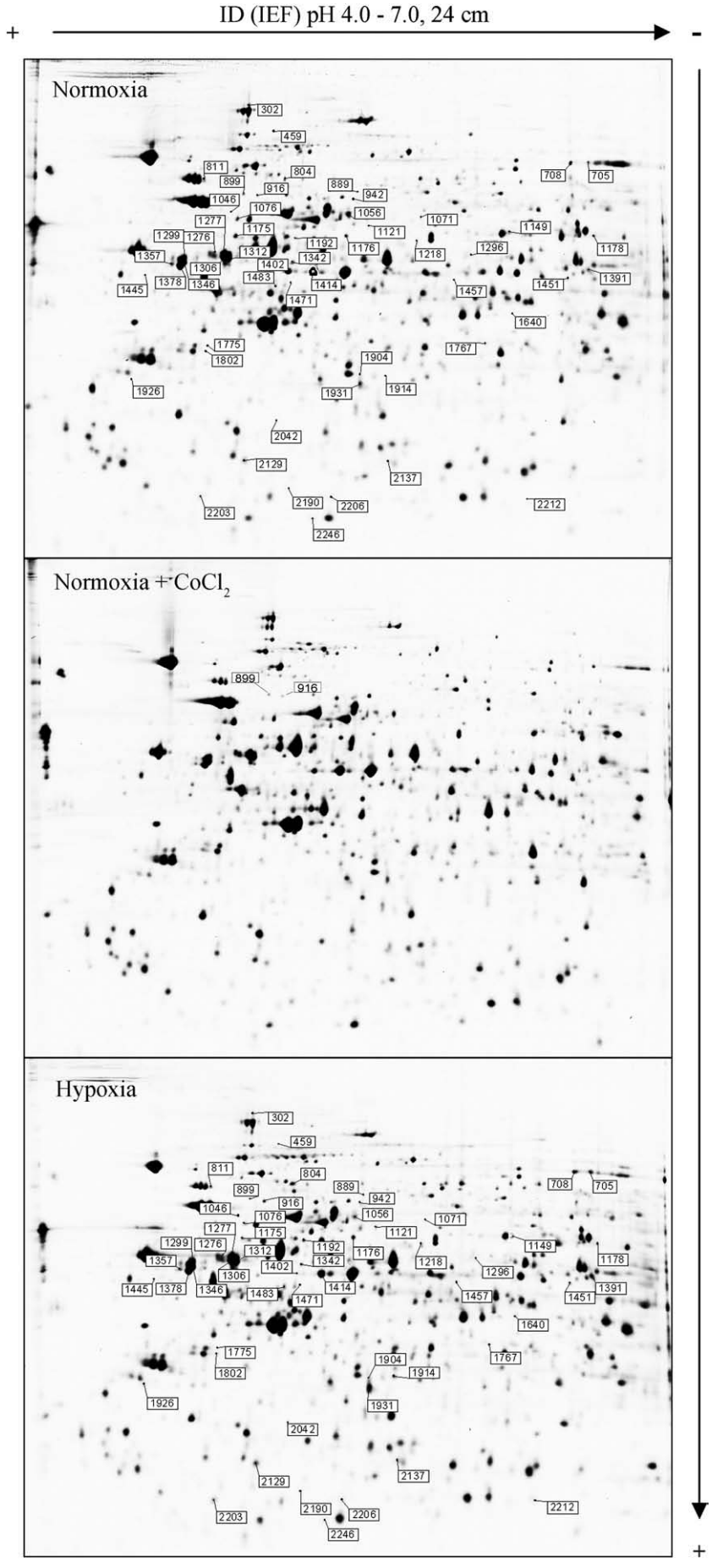
ID (IEF) pH 4.0 - 7.0, 24 cm
+
-
Normoxia
302
459
811
804
899
889
916
942
708
705
1046
1076
1056
1277
1071
1175
1121
1149
1299
1276
1192
1176
1296
1178
1357
1312
1342
1218
1306
1402
1483
1391
1445
1378
1346
1414
1457
1451
1471
1640
1775
1767
1802
1904
1926
1931
1914
2042
2129
2137
2190
2206
2203
2212
2246
Normoxia + CoCl2
899
916
Hypoxia
302
459
811
804
899
889
916
942
708
705
1046
1076
1056
1277
1071
1175
1121
1149
1299
1276
1312
1192
1176
1178
1357
1342
1218
1402
1296
1306
1445
1378
1346
1483
1414
1457
1451
1391
1471
1640
1775
1904
1767
1802
1914
1926
1931
2042
2137
2129
2190
2206
2212
2203
2246
+

2.2.18. Statistical analysis

One way analysis of variance (ANOVA) with post-hoc pairwise comparison using Holm–Sidak method was performed using SigmaStat.3 software.

3. Results

3.1. 2D-DIGE analysis, experimental procedure and mass spectrometry

In order to identify HIF-1 independent proteins involved in the adaptive response to hypoxia, we used the murine hepatoma cell line HepaC4, which lacks ARNT, and hence, does not harbor a functional HIF-1. Cells were first incubated during 16 h under normoxia or hypoxia. After lysis, proteins were labeled with different dyes to perform 2D-DIGE approach and the gels were analyzed by the DeCyder software [32]. We decided to focus on proteins that had their relative abundance statistically modified at least by 50% under hypoxia in comparison to normoxia ($p = 0.05$).

A total of 21 hypoxia-responsive proteins were identified by mass spectrometry (Table 1). Most of them were clustered into cytoskeleton or associated to cytoskeleton proteins (like vimentin, cortactin, DH IC-2 and lamin). We then tried to confirm these variations using Western blot analyses. However, no correlation between the apparent modification of abundance observed in 2D-DIGE and the abundance of the proteins was observed. Real-time PCR, to assay the mRNA level, and immunofluorescence, to evidence changes in abundance and in subcellular localization, did not neither reveal any variation (data not shown).

In order to circumvent this problem, we decided to use the same kind of approach using a closely related human hepatoma cell line, the HepG2 cells. We decided to compare the protein profile of cells incubated under hypoxia to the one of cells incubated in the presence of $CoCl_2$ under normoxia. Hypoxia allowed us to identify HIF-1 dependent and independent hypoxia-responsive proteins while $CoCl_2$ only highlighted the HIF-1 dependent ones. We next removed the common proteins of both experiments and generated a list of HIF-1 independent hypoxia-responsive proteins. To optimize our chances to identify proteins common with the previous experiment, we focused our attention on proteins that had their relative abundance changed at least by 30% under hypoxia. Normoxia was used as the control.

First, to confirm that HepG2 cells are responsive to $CoCl_2$, we checked the stabilization of HIF-1α under normoxia in the presence of $CoCl_2$ or under hypoxia after 16 h incubation (data not shown). Hypoxia and $CoCl_2$ did indeed lead to an increase in HIF-1α protein level. Second, we carried out 2D-DIGE approach where HepG2 cells were incubated under normoxia, normoxia with $CoCl_2$ or hypoxia for 16 h. Fig. 1 illustrates the protein spots resolved by two-dimensional electrophoresis for the three experimental conditions used here. After comparison of the hypoxic and $CoCl_2$-induced protein profiles, common spots were removed and we generated a list of 77 spots responsive to hypoxia in a HIF-1 independent manner. Out of these spots, 63 proteins were identified by mass spectrometry and clustered into different groups: cytoskeleton or cytoskeleton-associated proteins (like coronin-1B, F-actin capping protein alpha-2 subunit and DH IC-2), proteins involved in translation process (like elongation factor 2, HNRPK, HNRPC and aconitase), stress proteins, kinases and so on (Table 2).

We decided to focus on cytoskeleton proteins for two major reasons. First, some of them were already identified in the preliminary experiment using HepaC4, like cortactin and DH IC-2. Second, these cytoskeleton proteins may be involved in the migration process, which is known to be enhanced under hypoxic conditions [33].

3.2. Increase in DH IC-2 protein level under hypoxia

In order to check whether the abundance of the different cytoskeleton proteins identified by mass spectrometry are indeed increased under hypoxia, HepG2 cells were incubated 16 h under hypoxia or normoxia. Then, cells were lysed and total cell extract proteins were loaded onto 10% SDS–PAGE. The abundance of five cytoskeleton proteins identified in the previous study was monitored by Western blot. The protein level of DH IC-2 was found to be increased under hypoxia as shown in Fig. 2A. The hypoxia-induced increase in DH IC-2 abundance was also confirmed by immunofluorescence (Fig. 2B), but no change in subcellular localization was observed. A time curve was also performed and the results show that DH IC-2 abundance began to increase already after 4 h of incubation under hypoxic conditions (Fig. 2C). All these experiments were performed at least three times (data not shown).

3.3. DH IC-2 mRNA level in HepG2 cells under hypoxia

To determine whether the DH IC-2 up-regulation observed under hypoxia is dependent on a transcriptional regulation, DH IC-2 mRNA level was quantitated by real-time PCR. HepG2 cells were incubated under hypoxia or normoxia in the presence or not of $CoCl_2$. Total mRNA was extracted and retrotranscripted into cDNA. Fig. 3 shows that neither hypoxia nor $CoCl_2$ did change the mRNA level of DH IC-2. On the other hand, both conditions did increase the mRNA level of aldolase, a well-known HIF-1 target gene (Fig. 3). These results indicate that it is probably not through enhanced transcription that the protein level of DH IC-2 is increased under hypoxic conditions.

3.4. DH IC-2 stabilization under hypoxia

In order to discriminate between protein stabilization and enhanced translation to explain the increased protein DH IC-2 expression under hypoxia, a time course analysis using cycloheximide 10 μM (CHX), a well-known inhibitor of mammalian cell translation [34], was performed under normoxia or hypoxia. As shown in Fig. 4A, when HepG2 cells were treated with CHX under hypoxia, the total amount of DH IC-2 did not diminish regardless of the incubation duration. There was rather an increase in DH IC-2 protein abundance. However, under normoxia, the level of DH IC-2 slightly decreased according to the duration of the time course experiment. These results suggest that, under hypoxia, the pool of DH IC-2 was stabilized, and this contributed to the accumulation of the protein. This effect may be due to an inhibition of the DH IC-2 degradation pathway under hypoxia. As proteasome is one of the major proteolytic systems of mammalian cells [35], we checked whether it could be involved in DH IC-2 degradation. To this aim, we used the proteasome inhibitor MG132 [36] at 40 μM under normoxia and the protein level of DH IC-2 was monitored by Western blot. As shown in Fig. 4B, DH IC-2 level was not modified under normoxia regardless of the incubating conditions, suggesting that another degradation pathway may be involved in DH IC-2 turn over. p53 was used as a positive control of proteasome inhibition. Its abundance indeed increased in the presence of MG132 (Fig. 4B).

3.5. DH IC-2 post-translational modification under hypoxia

Since changes in 2D gel spots may be due to changes in expression but also in post-translational modification, we checked if DH IC-2 would also be post-translationally modified under hypoxia. 2D-blot analyses were performed on proteins from HepG2 cells incubated under the three different conditions. As shown in Fig. 5, DH IC-2 was detected as two distinct spots under normoxia and after the incubation in the presence of $CoCl_2$. However, under hypoxia, only one spot remained. These results suggest that DH IC-2 is modified under hypoxia. Similar results were obtained for other cytoskeleton proteins like tubulin, cortactin and coronin-1B (data not shown). The DH IC-2 shift observed by 2D-blot under hypoxia, from the more acidic form to the less one, may correspond to a loss of negative

Table 2
List of HIF-1 independent hypoxia-responsive proteins identified by mass spectrometry in HepG2 cells.

Master no.	Name	T-test	Av. Ratio	pI	Mw	Pept.	Protein ID	Comment
302	Oxygen-regulated protein precursor	0.0017	−1.6	4.97	111266	19	Q9Y4L1	Role in cytoprotective cellular mechanisms triggered by oxygen deprivation and other stresses as a molecular chaperone. Participates in protein folding.
459	Kinectin variant 1	0.026	1.9	5.36	156178	5	Q86UP2	Involved in kinesin-driven vesicle motility.
556*	Ubiquitin-protein ligase E1	0.018	2.86	8.77	21404	29	P51965	Mediates the selective degradation of short-lived and abnormal proteins.
705	Elongation factor 2	0.0067	1.64	6.49	95277	6	P13639	Promotes the GTP-dependent translocation of the nascent protein chain from the A-site to the P-site of the ribosome.
708	Elongation factor 2	0.00096	1.58	6.49	95277	4	P13639	Promotes the GTP-dependent translocation of the nascent protein chain from the A-site to the P-site of the ribosome.
708	Aconitase 1	0.00096	1.58	6.22	98336	9	Q5VZA7	Cofactor, binds 4Fe-4S.
708	Molybdenum cofactor sulfurase	0.00096	1.58	6.24	98067	2	Q96EN8	Sulfurates the molybdenum cofactor.
708	P1-CDC21	0.00096	1.58	6.27	96497	10	P33991	Involved in the control of DNA replication.
804	Cortactin isoform a	0.0019	2.53	5.07	61548	13	Q96H99	Involved in organization of cell structure. May contribute to cellular growth regulation and transformation.
811	HSP90 beta	0.0037	1.92	4.77	83212	28	P08238	Molecular chaperone.
889	eIF-4b	3.40E-05	4.78	5.3	69183	1	P23588	Required for the binding of mRNA to ribosomes.
899	Dynein intermediate chain 2C	0.0041	−3.99	5.08	71456	2	Q13409-3	Helps dynein bind to dynactin.
916	Dynein intermediate chain 2C	7.30E-05	2.74	5.08	71456	10	Q13409-3	Helps dynein bind to dynactin.
942	Cytokeratin 10	0.00012	2.54	4.95	59482	5	Q14664	Intermediate filament.
942	Prothrombin precursor	0.00012	2.54	5.52	69992	3	P00734	Cleaves bonds after Arg and Lys. Involved in blood homeostasis, inflammation and wound healing.
942	Aglucosidase alpha	0.00012	2.54	5.56	10527	4	Q09GN4	Essential for the degradation of glygogen to glucose in lysosomes.
1046	alpha tubulin	0.00078	1.64	5.76	49895	2	Q9BQE3	Component of microtubules.
1056	Dihydrolipoamide acetyltransferase	8.00E-05	−1.96	5.97	65674	3	Q16783	Part of the pyruvate dehydrogenase complex, which catalyzes the overall conversion of pyruvate to acetyl-CoA and CO_2.
1056	alpha-fetoprotein precursor	8.00E-05	−1.96	5.3	68633	3	P02771	Binds copper, nickel, fatty acids and bilirubin less than serum albumin.
1071	Serum albumin	0.00035	−2.77	6.09	69348	3	P02768	Main protein of plasma, has a good binding capacity for water, Ca(2+), Na(+), K(+), fatty acids, hormones, bilirubin and drugs. Involved in the regulation of the colloidal osmotic pressure of blood.
1076	Lamin B1	0.013	−1.55	4.91	66367	19	P20700	Component of the nuclear lamina.
1121	Coronin 1B	0.00089	1.41	5.5	54200	5	Q9BR76	Regulates leading edge dynamics and cell motility in fibroblasts. May be involved in cytokinesis and signal transduction.
1121	Ras-GTPase activating protein binding protein 1	0.00089	1.41	5.2	52132	1	Q13283	May be a regulated effector of stress granule assembly.
1149	Dihydropyrimidinase-like 2	0.027	1.34	5.92	62254	6	Q53ET2	Involved in the metabolism of cyclic imides.
1175	HNRPK	0.012	−1.99	5.22	50944	13	Q07244	Pre-mRNA-binding proteins.
1175	Cytokeratin 9	0.012	−1.99	5.01	62091	6	Q14665	Plays a role in keratin filament assembly.
1175	TRAP1	0.012	−1.99	8.2	80059	1	Q12931	Chaperone.
1176	ERO1-L alpha	0.002	1.38	5.35	54358	2	Q96HE7	Oxidizes proteins in the endoplasmic reticulum to produce disulfide bonds.
1176	Myo-inositol 1-phosphate synthase 1	0.002	1.38	5.4	61029	5	Q9NPH2	Involved in myo-inositol biosynthesis pathway that catalyzes the conversion of glucose 6-phosphate to 1-myo-inositol 1-phosphate in a NAD-dependent manner.
1176	Copine-1	0.002	1.38	5.52	59058	9	Q99829	May function in membrane trafficking.
1178	Lamin A/C	0.0063	1.35	6.58	74070	8	Q5I6Y4	Component of the nuclear lamina.
1192	HNRPK	0.021	1.58	5.22	50944	7	Q07244	Pre-mRNA-binding proteins.
1218	p21-activated kinase 2	0.00026	1.45	5.59	57967	4	Q13177	Phosphorylates ribosomal protein S6, histone H4 and myelin basic protein. Full-length PAK 2 stimulates cell survival and cell growth.
1276	PDI	0.037	1.85	4.56	57080	6	Q15205	Catalyzes the formation, breakage and rearrangement of disulfide bonds. Also acts a structural subunit of various enzymes such as prolyl 4-hydroxylase and microsomal triacylglycerol transfer protein MTTP.
1277	alpha tubulin	0.0091	1.57	5.76	49895	10	Q9BQE3	Component of microtubules.
1277	PDI	0.0091	1.57	4.57	57081	10	Q15205	Catalyzes the formation, breakage and rearrangement of disulfide bonds. Also acts a structural subunit of various enzymes such as prolyl 4-hydroxylase and microsomal triacylglycerol transfer protein MTTP.
1289*	alpha tubulin	0.013	1.59	5.76	49895	15	Q9BQE3	Component of microtubules.
1296	DEAD box protein 19A	0.012	1.59	6.16	53940	7	Q9NUU7	ATP-dependent RNA helicase involved in mRNA export from the nucleus.
1296	Glycerokinase	0.012	1.59	5.89	57542	6	Q8IVR5	Key enzyme in the regulation of glycerol uptake and metabolism.

(continued on next page)

Table 2 *(continued)*

Master no.	Name	T-test	Av. Ratio	pI	Mw	Pept.	Protein ID	Comment
1299	beta 2 tubulin	0.024	1.75	4.6	49799	19	P68371	Component of microtubules.
1299	MAPK7 transcript variant 5	0.024	1.75	6.7	50360	1	Q59F50	Splice variant of ERK5. Lacks the NLS sequence and the prolinerich domain.
1306	alpha tubulin	0.044	1.31	5.76	49895	12	Q9BQE3	Component of microtubules.
1312	beta 1 tubulin	0.034	1.35	5.76	49895	1	Q9BQE3	Component of microtubules.
1342	FKBP4	0.0015	−1.64	5.18	51772	4	Q02790	Component of unactivated mammalian steroid receptor complexes that sediment at 8-10 S. May have a rotamase activity. May play a role in the intracellular trafficking of hetero-oligomeric forms of steroid hormone receptors.
1346	beta 2 tubulin	0.0052	1.38	4.6	49799	24	P68371	Component of microtubules.
1357	beta 5 tubulin	0.049	1.86	4.55	49726	13	P07437	Component of microtubules.
1378	beta tubulin	0.0032	1.46	4.5	47736	16	Q5JP53	Component of microtubules.
1391	Heterogeneous nuclear ribonucleoprotein H1	0.0097	1.34	5.85	49198	5	P31943	Component of the heterogeneous nuclear ribonucleoprotein (hnRNP) complexes which provide the substrate for the processing events that pre-mRNAs undergo before becoming functional, translatable mRNAs in the cytoplasm.
1402	alpha tubulin	0.00069	−7.19	5.76	49895	4	Q9BQE3	Component of microtubules.
1402	Cytokeratin 8	0.00069	−7.19	5.52	53704	20	Q14099	Helps to link the contractile apparatus to dystrophin at the costameres of striated muscle.
1402	beta 5 tubulin	0.00069	−7.19	4.55	49726	2	P07437	Component of microtubules.
1414	Cytokeratin 8	0.0011	−2.88	5.52	53704	19	Q14099	Helps to link the contractile apparatus to dystrophin at the costameres of striated muscle.
1445	Cytokeratin 10	0.014	1.44	5.13	59510	2	Q14664	Intermediate filament.
1445	alpha tubulin	0.014	1.44	5.76	49895	3	Q9BQE3	Component of microtubules.
1451	CSTF 50	0.0012	1.39	6.115	48326	8	Q05048	Required for polyadenylation and 3′-end cleavage of mammalian pre-mRNAs. May be responsible for the interaction of CSTF with other factors to form a stable complex on the pre-mRNA.
1457	Rho GTPase activating protein 1	0.048	1.34	5.82	50404	4	Q07960	GTPase activator for the Rho, Rac and Cdc42 proteins, converting them to the putatively inactive GDP-bound state.
1471	DNA polymerase delta subunit 2	0.041	1.69	5.21	51257	2	P49005	The function of the small subunit is not yet clear.
1483	Proteasome 26 s non ATPase subunit 5	0.00088	1.59	5.3	56559	5	Q16401	Belongs to the 26S multi-subunit protease, which is required for ubiquitin-dependent proteolysis.
1640	MAPKK2	0.0014	2.29	6.09	44396	4	P36507	Catalyzes the concomitant phosphorylation of a threonine and a tyrosine residue in a Thr-Glu-Tyr sequence located in MAP kinases. Activates the ERK1 and ERK2 MAP kinases.
1767	HNRPA/B	0.0029	−2.02	9.5	31327	2	Q99729	Binds single-stranded RNA.
1775	HNRPC	0.00012	3.16	4.8	32373	3	Q53EX2	Binds pre-mRNA and nucleates the assembly of 40S hnRNP particles. Interacts with poly-U tracts in the 3′-UTR or 5′-UTR of mRNA and modulates the stability and the level of translation of bound mRNA molecules.
1802	HNRPC	9.30E-05	3.34	4.8	32373	2	Q53EX2	Binds pre-mRNA and nucleates the assembly of 40S hnRNP particles. Interacts with poly-U tracts in the 3′-UTR or 5′-UTR of mRNA and modulates the stability and the level of translation of bound mRNA molecules
1848	eIF-2a	0.00033	1.44	4.82	36089	3	P05198	Functions in the early steps of protein synthesis by forming a ternary complex with GTP and initiator tRNA.
1904	F-actin capping protein alpha-2 subunit	0.013	1.5	5.47	32928	3	P47755	Binds in a Ca(2+)-independent manner to the fast growing ends of actin filaments (barbed end) thereby blocking the exchange of subunits at these ends.
1914	RPLPO	0.00072	2.72	8.43	27281	6	Q6NSF2	Component of the ribosome complex.
1926	SGTA	0.00035	2.04	4.59	34041	10	Q9BTZ9	Co-chaperone that binds directly to HSC70 and HSP70 and regulates their ATPase activity.
1926	Nucleophosmin	0.00035	2.04	4.47	32439	2	Q12826	Associated with nucleolar ribonucleoprotein structures and bind single-stranded nucleic acids. May function in the assembly and/or transport of ribosome.
1931	SULT1A3	0.01	1.48	5.6	34174	1	Q6ZWJ5	Catalyzes the sulfate conjugation of phenolic monoamines (neurotransmitters such as dopamine, norepinephrine and serotonin) and phenolic and catechol drugs.
2042	Proteasome inhibitor PI31 subunit	0.0007	1.3	5.32	29753	2	Q92530	Plays an important role in control of proteasome function. Inhibits the hydrolysis of protein and peptide substrates by the 20S proteasome.
2042	Copper chaperone for superoxide dismutase	0.0007	1.3	5.02	29022	4	Q2M366	Delivers copper to copper zinc superoxide dismutase (SOD1).
2129	RanBP1	0.0068	1.37	5.02	23295	1	P43487	Inhibits GTP exchange on Ran. Forms a Ran-GTP-RANBP1 trimeric complex. Increases GTP hydrolysis induced by the Ran GTPase activating protein RANGAP1. May act in an intracellular signaling pathway which may control the progression through the cell cycle by regulating the transport of protein and nucleic acids across the nuclear membrane.
2137	Guanidinoacetate N-methyltransferase	0.013	1.38	5.7	26301	3	Q14353	Involved in amine, polyamine and creatine biosynthesis.
2190	ITPA	0.011	1.36	5.35	21431	3	Q9BY32	May be the major enzyme responsible for regulating ITP concentration in cells.

Table 2 *(continued)*

Master no.	Name	T-test	Av. Ratio	pI	Mw	Pept.	Protein ID	Comment
2203	Catechol O-methyl transferase	0.00026	1.57	5.11	30017	3	Q6IB07	Catalyzes the O-methylation, and thereby the inactivation of catecholamine neurotransmitters and catechol hormones.
2206	UMP-CMP kinase	0.00049	1.36	5.26	22208	6	Q53GB7	Catalyzes specific phosphoryl transfer from ATP to UMP and CMP.
2212	Lysophospholipase 1	0.028	1.59	6.31	24653	4	Q9UQF9	Hydrolyzes fatty acids from S-acylated cysteine residues in proteins such as trimeric G alpha proteins or HRAS. Has also a low lysophospholipase activity.
2212	BAG-2 (BCL2-associated athanogene 2)	0.028	1.59	6.25	23757	3	Q08AS9	Inhibits the chaperone activity of HSP70/HSC70 by promoting substrate release.
2246	Adenine phosphoribosyltransferase	0.014	1.32	5.65	19595	2	Q3KP55	Catalyzes a salvage reaction resulting in the formation of AMP, that is energically less costly than de novo synthesis.

HepG2 cells were incubated 16 h under hypoxia or normoxia and $CoCl_2$. Normoxia was used as the control. Hypoxia-responsive HIF-1 independent proteins were selected and then identified by mass spectrometry using a Nano-LC-QTOF-MSMS coupled to the MassLynx 4.0 software. Full-length proteins were identified with Mascot software (version 2.0) by sequence homology research against human protein databases. T-test = Student's *t* test ($p<0.05$); Av. Ratio = biological variation in induction fold; pI = isoelectric point; Mw = molecular weight; Pept. = numbers of matching peptides. * = protein identified by MALDI coupled to the MassLynx 4.0 software. Full-length proteins were also identified with Mascot software (version 2.0) by sequence homology research against human protein databases.

charges or a gain of positive ones. It may reflect, for example, a loss of phosphorylation or of acetylation of this protein under hypoxia. *In silico* research pointed out several potential phosphorylation sites in the DH IC-2 protein sequence (data not shown). The intensity of the spot detected under hypoxia by 2D-blot analysis should be more than the sum of the two spots detected under normoxia. It is however possible that the affinity of the antibody for the unphosphorylated form would not be the same as its affinity for the phosphorylated form, that would explain our results.

In order to confirm that the change in the phosphorylation state of DH IC-2 was independent of HIF-1, HIF-1α was invalidated using siRNA. Fig. 6 shows that while HIF-1α protein abundance was markedly decreased, HIF-1α invalidation did not influence the effect of hypoxia on the modification of DH IC-2 observed on 2D-blot.

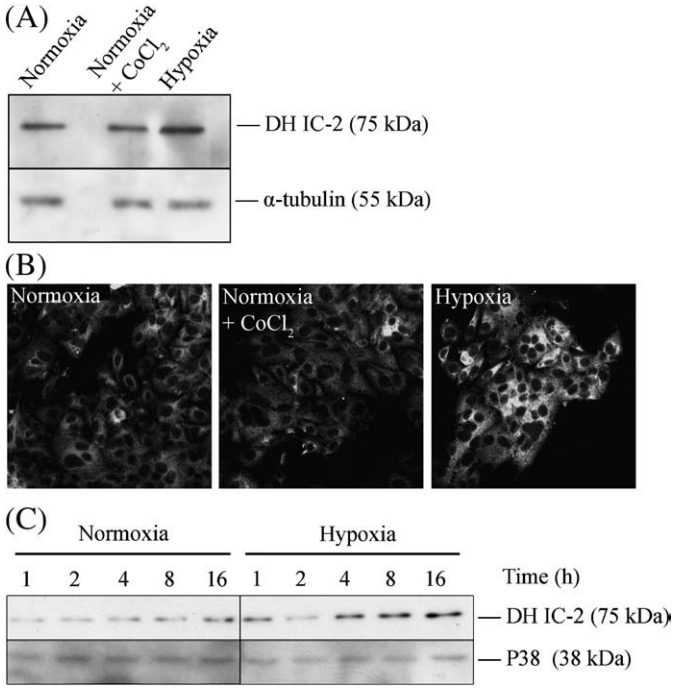

Fig. 2. Effect of hypoxia on DH IC-2 abundance and subcellular localization. (A) HepG2 cells were incubated 16 h under normoxia, normoxia + $CoCl_2$ 150 μM or hypoxia. Total cell lysates were run on SDS–PAGE (10%) and probed with anti-DH IC-2 specific IgG. α-Tubulin was used as loading control. (B) After incubation, cells were fixed, permeabilized and labeled with anti-DH IC-2 specific IgG. Observations were made using a confocal microscope with a constant photomultiplier. (C) HepG2 cells were incubated increasing time under normoxia or hypoxia. Total cell lysates were run on SDS–PAGE (10%) and probed with anti-DH IC-2 specific IgG. p38 was used as loading control.

In order to identify the putative kinase responsible for the phosphorylation of DH IC-2 under normoxia, we performed immunoprecipitation studies. Cells were first treated with inhibitors of different kinases (calphostin C for PKC, DRB for CK2 and SB203580 for p38) under normoxic conditions or incubated in the presence of $CoCl_2$ or under hypoxia and were then lysed. DH IC-2 was immunoprecipitated from the lysates, run onto a SDS–PAGE gel and revealed with an anti-phosphorylated pan-serine-threonine antibody. The results show that DH IC-2 was indeed phosphorylated under normoxic conditions, $CoCl_2$ did not influence it while hypoxia strongly inhibited this phosphorylation (Fig. 7A). Moreover, under normoxia, the phosphorylation was inhibited in the presence of calphostin C, a PKC inhibitor, but not when CK2, p38 (Fig. 7A) or ERK (data not shown) was inhibited. In order to confirm these results, 2D-blot analyses were performed on proteins from HepG2 cells incubated under normoxia with or without calphostin C. As shown in Fig. 7B, calphostin C markedly decreased the abundance of the more acidic spot while in parallel it increased the abundance of the less acidic one, which is similar to what was observed under hypoxia (see Fig. 5). All together, these results suggest that DH IC-2 is phosphorylated by PKC under normoxia and that hypoxia inhibited this post-translational modification.

In order to support this hypothesis, actual PKC activity was assayed. Results from Fig. 7C show that hypoxia significantly decreased PKC activity, while $CoCl_2$ had no effect. PMA, used as a positive control, strongly increased PKC activity. It must be noted that

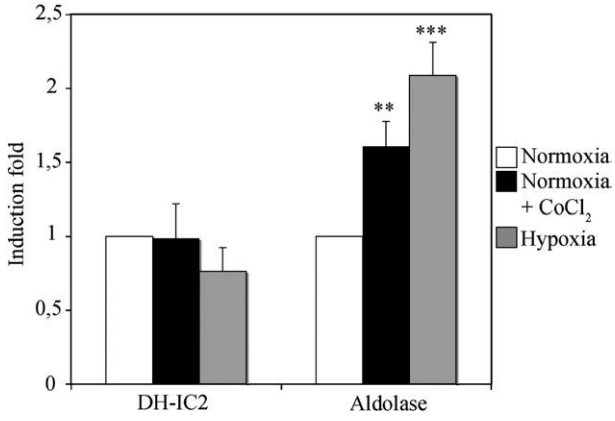

Fig. 3. Effect of hypoxia on DH IC-2 and aldolase mRNA level. HepG2 cells were incubated 16 h under normoxia, normoxia + $CoCl_2$ 150 μM or hypoxia. After incubation, total RNA was extracted, retrotranscribed into cDNA and submitted to real-time PCR for DH IC-2 and aldolase. Rpl13 was used as housekeeping gene. The results are expressed in induction fold for three independent experiments, as means ± SD ($n=3$). ** or *** $p<0.01$ or $p<0.001$ vs. normoxia.

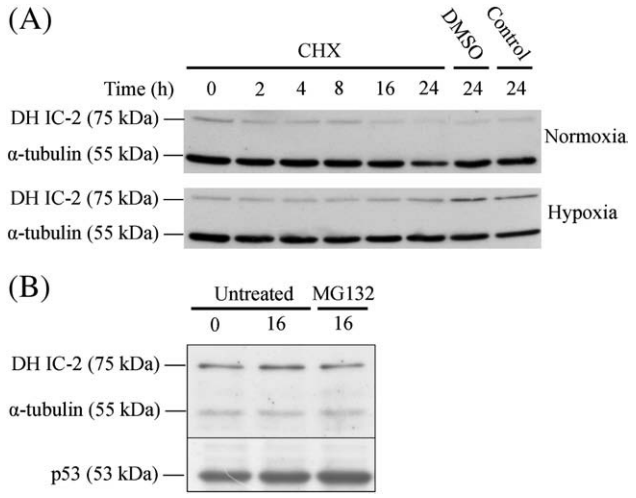

Fig. 4. DH IC-2 stabilization under hypoxia. (A) HepG2 cells were incubated under normoxia or hypoxia in a time course experiment in the presence of cycloheximide 10 μM (CHX). Total cell lysates (40 μg) were run on SDS–PAGE (10%) and probed with anti-DH IC-2 specific IgG. The abundance of DH IC-2 was quantified and plotted. (B) Effect of proteasome inhibition on DH IC-2 protein level. HepG2 cells were incubated under normoxia in the presence or absence of MG132 (40 μM) during 16 h. Total cell lysates (40 μg) were run on SDS–PAGE (10%) and probed with anti-DH IC-2 specific IgG. p53 was used to monitor proteasome inhibition and α-tubulin was used as loading control.

the effect of calphostin C on PKC activity could not be measured because it interfered with the measure of the optical density. These data suggest that hypoxia may inhibit PKC activity after 16 h of incubation.

3.6. DH IC-2 and migration

As DH IC-2 and other cytoskeleton proteins are modified under hypoxia, we decided to investigate the possibility that these modifications may affect cellular migration. For this purpose, DH IC-2 was invalidated in HepG2 cells by the use of siRNA. As a first step, we checked, in a time course experiment, that expression of DH IC-2 was knocked-down after cell transfection in the presence of the siRNA. As shown in Fig. 8, total invalidation of DH IC-2 was achieved 24 h post-transfection and remained stable at least until 72 h post-transfection.

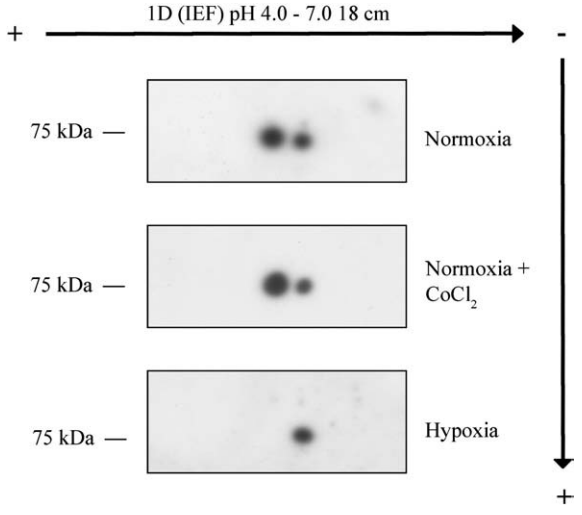

Fig. 5. Post-translational modification of DH IC-2 under hypoxia. HepG2 cells were incubated 16 h under normoxia, normoxia + $CoCl_2$ 150 μM or hypoxia. After incubation, 100 μg of total cell lysates were loaded on 18 cm IEF pH 4–7 strip. After the first dimension, proteins were separated on 10% SDS–PAGE and transferred on polyvinyldiene difluoride membrane. Proteins were detected with anti-DH IC-2 specific IgG.

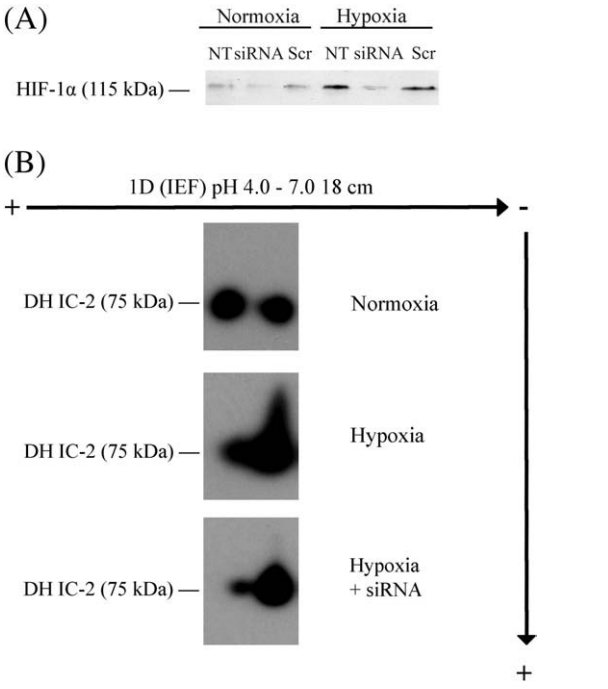

Fig. 6. Effect of HIF-1α invalidation on DH IC-2 hypoxia-induced modification. (A) HepG2 cells were transfected with HIF-1α-directed siRNA for 24 h (NT = non-transfected, Scr = non-targeting siRNA, HIF-1α siRNA = HIF-1α siRNA smartpool). HepG2 cells were re-plated 24 h post-transfection and, 1 day later, incubated 8 h under normoxia and hypoxia. Each sample (40 μg) was run on SDS–PAGE (10%) and probed with anti-HIF-1α specific IgG. (B) HepG2 cells were first transfected with HIF-1α-directed siRNA for 24 h. After, HepG2 cells were re-plated 24 h post-transfection and, 1 day later, incubated 24 h under hypoxia. In parallel, non-transfected HepG2 cells were incubated 16 h under normoxia or hypoxia. After incubation, 100 μg of each total cell lysate were loaded on 18 cm IEF pH 4–7 strip. After the first dimension, proteins were separated on 10% SDS–PAGE and transferred on polyvinyldiene difluoride membrane. Proteins were detected with anti-DH IC-2 specific IgG.

We decided to perform the experiments between 24 and 48 h post-transfection, according to the type of the assay. In order to observe the impact of DH IC-2 invalidation on cell migration, transfected HepG2 cells were seeded on the top of porous membrane of Boyden-like chambers. The chambers were then incubated either under normoxia or hypoxia for 24 h. As shown in Fig. 9, HepG2 cells showed a higher migration when incubated under hypoxia. This result is in accordance with different *in vitro* and *in vivo* data from the literature, which show an increase in metastatic potential in hypoxic cancers [9,37]. We also observed, that under normoxia, HepG2 cells transfected with DH IC-2 targeting siRNA had a much more potent capacity to migrate through the porous membrane than control cells. Under hypoxia, this difference was attenuated. Under hypoxia, the total abundance of DH IC-2 is increased and the protein is no longer phosphorylated. In these conditions, HepG2 migration is enhanced. Two hypotheses can thus be put forward: (i) it is the abundance of DH IC-2 that regulates migration or (ii) that is the fact that DH IC-2 is phosphorylated or not. Since when DH IC-2 expression is lowered (by the use of siRNA), migration is also enhanced, we concluded that it is not its abundance that regulates migration (otherwise we should have observed an inhibition). We thus proposed that the phosphorylated form inhibits migration, while the unphosphorylated one favors migration: hypoxia, by inhibiting PKC activity and, hence, DH IC-2 phosphorylation would thus enhance cell migration. In order to confirm this hypothesis, we used calphostin C, a specific PKC inhibitor: under normoxia, PKC inhibition also resulted in an enhanced migration as hypoxia did (Fig. 10A and B). The effect of calphostin C was similar to the one of hypoxia, i.e., an increase in cell migration but the extent of the effect was lower. This may be due to the fact that migration may be regulated by several pathways under hypoxia, one of them being

PKC which is inhibited by calphostin C but the others would not be inhibited. In conclusion, hypoxia enhances migration at least in part by inhibiting DH IC-2 phosphorylation. These results suggest that DH IC-2 may be implicated in regulating the migration process, with a negative impact on migration in well-oxygenated conditions.

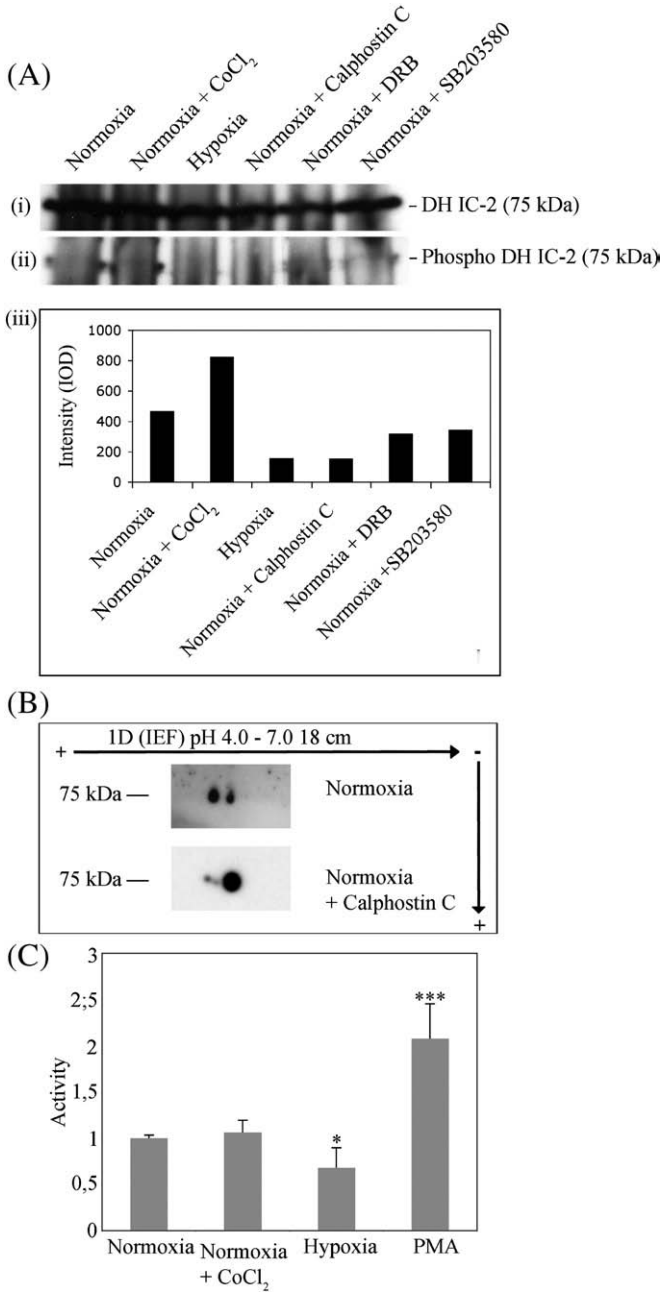

Fig. 7. Inhibition of DH IC-2 phosphorylation under hypoxia. (A) HepG2 cells were incubated 16 h under normoxia, normoxia + $CoCl_2$ 150 μM, normoxia + calphostin C 2 μM, normoxia + DRB 100 μM, normoxia + SB203580 20 μM or hypoxia. After DH IC-2 immunoprecipitation, an equal part of the purified lysates was run on separate SDS–PAGE (10%) and probed with anti-DH IC-2 specific IgG (i) or pan-anti-serine/threonine IgG (ii). The abundance of the phosphorylated form of DH IC-2 has been quantified and plotted (iii). (B) HepG2 cells were incubated 16 h under normoxia or normoxia + calphostin C 2 μM. After incubation, 100 μg of total cell lysates were loaded on 18 cm IEF pH 4–7 strip. After the first dimension, proteins were separated on 10% SDS–PAGE and transferred on polyvinyldiene difluoride membrane. Proteins were detected with anti-DH IC-2 specific IgG. (C) HepG2 cells were incubated 16 h under normoxia, normoxia + $CoCl_2$ 150 μM or hypoxia. A positive control using PMA stimulation at 0.3 μM for 7 min was also performed. After incubation, 20 μg of total cell lysates were used in ELISA to monitor pan-PKC activity. Optical density was measured at 495 nm. Results are presented as means ± SD ($n = 3$). * or ***, $p < 0.05$ or $p < 0.001$ vs. normoxia.

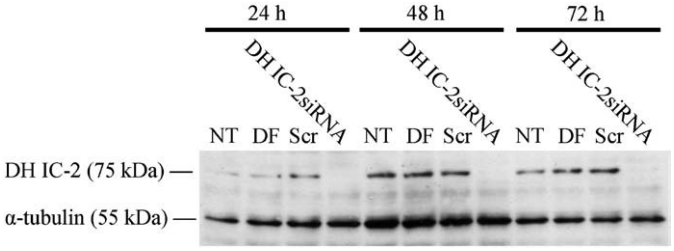

Fig. 8. Effect of DH IC-2-directed siRNA transfection on DH IC-2 protein level. HepG2 cells were transfected with DH IC-2-directed siRNA for 24 h (NT = non-transfected, DF = Dharmafect 1 transfection agent, Scr = non-targeting siRNA, DH IC-2 = DH IC-2 siRNA smartpool). Total cell lysates were collected 24, 48 or 72 h post-transfection. Each sample (40 μg) was run on SDS–PAGE (10%) and probed with anti-DH IC-2 specific IgG. α-Tubulin was used as loading control.

In parallel with the migration experiments, transfected HepG2 cells were seeded to perform proliferation assays, and incubated under normoxia or hypoxia during 24 h. Cell density was estimated by the MTT method. As shown in Fig. 11, invalidation of DH IC-2 did not change HepG2 cell proliferation rate. Taken together, these results showed that cell migration is enhanced by hypoxia and, to the same extent, by DH IC-2 invalidation in a ce:paraproliferation-independent way.

4. Discussion

Cancer represents one of the major causes of mortality in developed countries. Today, tumor hypoxia is a hot spot in cancer research and its impact on cancer development and patient outcome is well described. As hypoxia is more often correlated with a poor prognosis for the patient [38], adaptive responses to hypoxia are intensively investigated. HIF-1 controls the majority of the genes induced by hypoxia [2] and most of the studies that try to impair cancer cell adaptation to hypoxia are focused on the HIF pathway [19]. However, some data clearly show that other factors may also participate to this adaptation, through a transcriptional effect or in other ways like protein interaction or post-translational modification [20–23]. Indeed, overexpression of a constitutive active form of HIF-1 does not recapitulate all the genes induced by hypoxia [20], and the invalidation of HIF-1 does not suppress the apoptosis protection observed under hypoxia, indicating that HIF-1 independent processes are involved [21]. In order to investigate these processes, we decided to identify proteins that participate to cellular adaptation to hypoxia in a HIF-1 independent way. We used the murine cell line HepaC4, which lacks the ARNT subunit of HIF-1 [39]. In that way, HepaC4 cells do not have a functional HIF-1 and can not transactivate HIF-1 target genes [40]. 2D-DIGE analyses were performed in order to identify hypoxia-responsive HIF-1 independent proteins, but no correlation was observed between the apparent overexpression pointed out in these analytical analyses and the mRNA or protein level of the putative candidates. These discrepancies between 2D-DIGE, real-time PCR and Western blot results are probably due to the fact that 2D-DIGE highlights post-translational modifications in addition to changes in overall expression. In order to increase the probability to identify some hypoxia-responsive HIF-1 independent proteins, new 2D-DIGE experiments using $CoCl_2$, a well-known inducer of HIF-1 [24], were carried out, using the human hepatoma cell line HepG2. These cells are sensitive to $CoCl_2$ and represent a well-established hypoxia model [8].

It is known that $CoCl_2$ may also affect other cellular functions than the HIF-1 pathway [41], but as we removed the results generated by this approach from the ones obtained with hypoxia, we did not increase the rate of false positives. However, it is possible that we excluded some hypoxia HIF-1 independent spots, due to a side effect of this molecule in a HIF-1 independent hypoxia-responsive pathway,

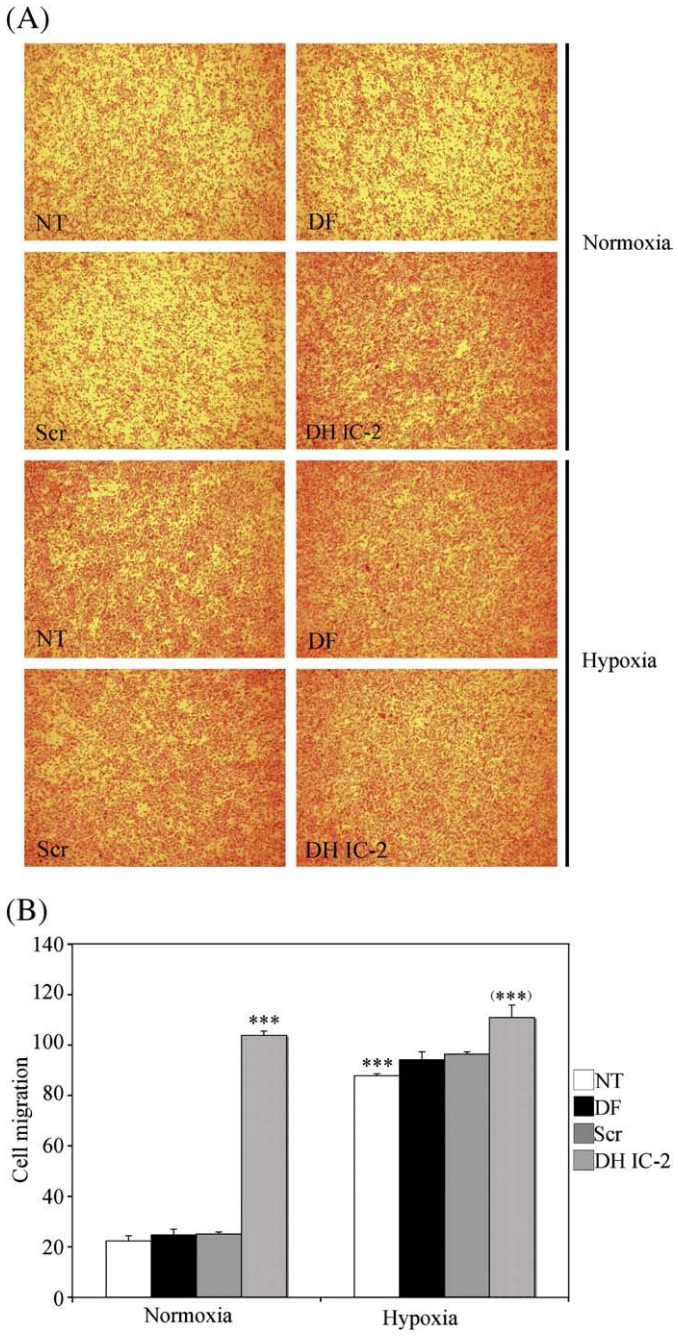

Fig. 9. Effect of DH IC-2 invalidation on HepG2 migration. HepG2 cells were transfected with DH IC-2-directed siRNA for 24 h (NT = non-transfected, DF = Dharmafect 1 transfection agent, Scr = non-targeting siRNA, DH IC-2 siRNA = DH IC-2 siRNA smartpool). HepG2 cells were re-plated in Boyden-like chambers 24 h post-transfection and incubated 24 h under normoxia and hypoxia. (A) Cells that have migrated were stained with crystal violet. (B) The actual number of cells that have migrated has been counted on three fields for each membrane of each experiment. The results are expressed in induction fold for three independent experiments, as means ± SD ($n = 3$). ***, $p < 0.001$ vs. normoxia; (***), $p < 0.001$ vs. hypoxia.

thus decreasing slightly the rate of true positives. After comparison of the lists of the different proteins identified by mass spectrometry in both experiments, we decided to focus on some cytoskeleton proteins for two major reasons. First, they were already identified in the previous experiments using the two murine cell lines. Second, they may be involved in regulating the migration process, which is known to be enhanced under hypoxic conditions. Out of these proteins, only the abundance of DH IC-2 was increased at the protein level. As DH IC-2 is a component of cytoplasmic dynein, which is involved in directed cell movement [42], we decided to focus on this protein. We first investigated if the increase in DH IC-2 protein level was dependent on a transcriptional effect. As DH IC-2 mRNA level was not elevated under hypoxia, we next investigated if the increase in DH IC-2 protein level may be the consequence of a stabilization of the protein. Blockage of protein synthesis by cycloheximide and follow-up of DH IC-2 protein level in a time course experiment revealed that this protein is less degraded under hypoxia. This result suggests that hypoxia-induced increase in DH IC-2 abundance is probably due to an accumulation of the protein rather than translational effect on the mRNA sequence. Under hypoxia, the overall protein synthesis is known to be slowed down following a limitation in ATP supply [43]. However, some mRNA (like VEGF) are still translated due to the presence of an IRES (internal ribosome entry site) sequence located in the 5′ untranslated region of the mRNA [44]. *In silico* analyses did not show such sequences in the DH IC-2 mRNA, leading to the conclusion that hypoxia-induced DH IC-2 overexpression is probably a consequence of the stabilization of this protein.

As post-translational modifications may increase the half-life of proteins, we next checked if DH IC-2 was altered by hypoxia. The results presented here clearly show that this protein is specifically modified under this condition. The shift observed by 2D-blot to a less acidic form of DH IC-2 suggests a loss of negative charges or a gain of positive ones. Different *in silico* analysis tools were used in order to define the potential modification involved in the DH IC-2 shift observed under hypoxia (data not shown). The NetPhos analysis pointed out putative phosphorylation sites and the immunoprecipitation studies showed that DH IC-2 is phosphorylated under normoxia and become de-phosphorylated under prolonged hypoxia (16 h). Calphostin C, a pan-inhibitor of PKC, also inhibited DH IC-2 phosphorylation while a decrease in PKC activity was observed after a prolonged incubation under hypoxia. We thus suggest that it is through PKC inhibition that hypoxia leads to the de-phosphorylation of DH IC-2 that we observed. HepG2 cells contain four PKC isoforms (α, δ, ε and ζ) [45]. Calphostin C inhibits all of them; further work is thus required to identify the actual isoenzyme responsible for DH IC-2 phosphorylation under normoxia. Several PCK isoenzymes have been found to be activated by short period of hypoxia in several cell types [46–48]. We postulate that prolonged hypoxia may lead to PKC deactivation through protein degradation as prolonged stimulation with PMA does [49], thus resulting in a decreased PKC activity. This hypothesis needs to be confirmed.

As proteasome 26 s is one of the major systems involved in protein turn over [35], we investigated if it could be implicated in DH IC-2 degradation. Proteasome activity was inhibited under normoxia by MG132 without any impact on DH IC-2 protein level suggesting that another pathway is in charge of its maintenance. Further work is needed to elucidate the mechanism involved in DH IC-2 degradation.

As we identified different cytoskeleton proteins, and as cytoplasmic dynein is involved in a variety of mechanisms like intracellular transport, mitosis, cell polarization and directed cell movement [28], which could be of particular interest in cancer progression, we decided to evaluate the implication of dynein on cancer cell migration. First, hypoxia was shown to enhance *in vitro* HepG2 cells mobility, which is in accordance with different literature data generated *in vitro* or *in vivo* [9,37]. Second, invalidation of DH IC-2 by siRNA increased HepG2 cell migration, to the same extent than hypoxia. The overall abundance of DH IC-2 is increased under hypoxia but the protein is no longer phosphorylated. In these conditions, HepG2 migration is increased. Two hypotheses can thus be put forward to explain these observations: (i) it is the abundance of DH IC-2 that regulates migration or (ii) it is the phosphorylation state of DH IC-2 that regulates migration. Since decreased DH IC-2 expression by siRNA enhanced cell migration, it is not its abundance that regulates migration. Indeed, if it would have been the case, an inhibition should

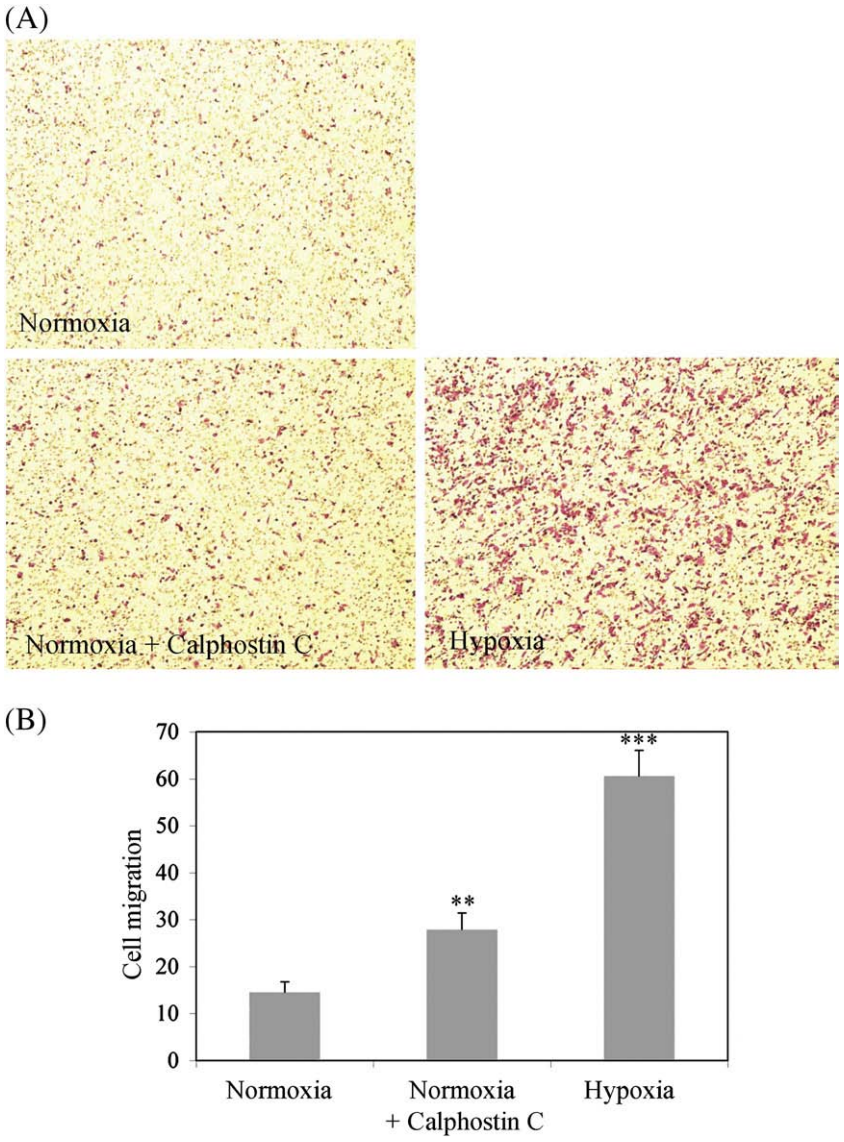

Fig. 10. Effect of pan-PKC inhibition on HepG2 migration. HepG2 cells were plated in Boyden-like chambers for 24 h and incubated under normoxia, normoxia + calphostin C at 2 μM or hypoxia. (A) Cells that have migrated were stained with crystal violet. (B) The actual number of cells that have migrated has been counted on three fields for each membrane of each experiment. The results are expressed in induction fold for three independent experiments, as means ± SD ($n = 3$). ** or ***, $p < 0.01$ or $p < 0.001$ vs. normoxia.

have been observed. We thus proposed that it is the phosphorylated form of DH IC-2 that inhibits migration, while the unphosphorylated one favors migration: hypoxia, by inhibiting PKC activity and, hence, DH IC-2 phosphorylation would thus enhance cell migration. We have confirmed this hypothesis using calphostin C, a specific PKC inhibitor: under normoxia, PKC inhibition also resulted in an enhanced migration. In conclusion, hypoxia enhances migration by inhibiting DH IC-2 phosphorylation. This effect was purely due to motility since there was no effect on cell proliferation. This last result is surprising, as dynein is known to play a role in spindle assembly [50]. However, as DH IC-2 is a multi-subunit complex protein, it is possible that DH IC-2 is not necessary for spindle assembly or could be replaced by a redundant protein.

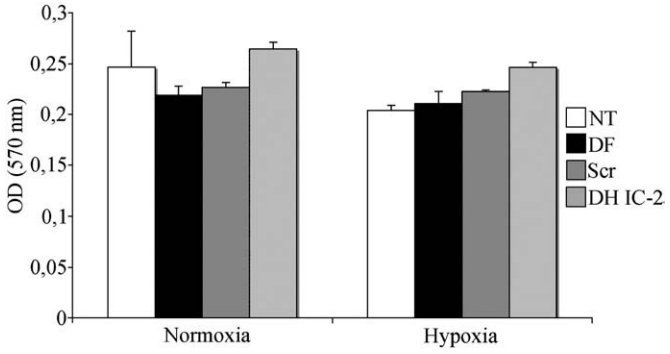

Fig. 11. Effect of DH IC-2 invalidation on HepG2 proliferation. HepG2 cells were transfected with DH IC-2-directed siRNA for 24 h (NT = non-transfected, DF = Dharmafect 1 transfection agent, Scr = non-targeting siRNA, DH IC-2 = DH IC-2 siRNA smartpool). HepG2 cells were re-plated 24 h post-transfection and, 1 day later, incubated 24 h under normoxia and hypoxia. Optical density was measured at 570 nm. Results are presented as means ± SD ($n = 4$).

Taken together, these results suggest that DH IC-2 is modified under hypoxia. This modification could disrupt dynein complex and, in turn, lead to the accumulation of DH IC-2 into the cytoplasm. As intermediate chains are crucial for dynein assembly and to monitor partner interactions [51,52], we hypothesized that the exclusion of this modified form of DH IC-2 may change the set of the dynein interacting proteins or may disturb normal dynein functions, enhancing cell migration. These results are important for understanding cancer development as they highlight a new HIF-1 independent mechanism involved in metastasis.

Acknowledgments

Sebastien Pyr dit Ruys is recipient of a FNRS-Télévie grant. Carine Michiels was research director of FNRS (Fonds National de la Recherche Scientifique, Belgium). The support of a FRFC grant from the FNRS is also acknowledged. This article presents results of the Belgian Program on Interuniversity Poles of Attraction initiated by the Belgian State, Prime Minister's Office, Science Policy Programming. The responsibility is assumed by its authors.

References

[1] G.L. Semenza, HIF-1: mediator of physiological and pathophysiological responses to hypoxia, J. Appl. Physiol. 88 (2000) 1474–1480.
[2] A.E. Greijer, P. van der Groep, D. Kemming, A. Shvarts, G.L. Semenza, G.A. Meijer, M.A. van de Wiel, J.A. Belien, P.J. van Diest, E. van der Wall, Up-regulation of gene expression by hypoxia is mediated predominantly by hypoxia-inducible factor 1 (HIF-1), J. Pathol. 206 (2005) 291–304.
[3] G.L. Semenza, L.A. Shimoda, N.R. Prabhakar, Regulation of gene expression by HIF-1, Novartis Found. Symp. 272 (2006) 2–8 discussion 8–14, 33–6.
[4] G.L. Wang, B.H. Jiang, E.A. Rue, G.L. Semenza, Hypoxia-inducible factor 1 is a basic-helix-loop-helix-PAS heterodimer regulated by cellular O2 tension, Proc. Natl. Acad. Sci. U. S. A. 92 (1995) 5510–5514.
[5] G.L. Semenza, Hydroxylation of HIF-1: oxygen sensing at the molecular level, Physiology (Bethesda) 19 (2004) 176–182.
[6] M.L. Whitelaw, J.A. Gustafsson, L. Poellinger, Identification of transactivation and repression functions of the dioxin receptor and its basic helix-loop-helix/PAS partner factor Arnt: inducible versus constitutive modes of regulation, Mol. Cell. Biol. 14 (1994) 8343–8355.
[7] H.P. Gerber, F. Condorelli, J. Park, N. Ferrara, Differential transcriptional regulation of the two vascular endothelial growth factor receptor genes. Flt-1, but not Flk-1/KDR, is up-regulated by hypoxia, J. Biol. Chem. 272 (1997) 23659–23667.
[8] J.P. Piret, E. Minet, J.P. Cosse, N. Ninane, C. Debacq, M. Raes, C. Michiels, Hypoxia-inducible factor-1-dependent overexpression of myeloid cell factor-1 protects hypoxic cells against tert-butyl hydroperoxide-induced apoptosis, J. Biol. Chem. 280 (2005) 9336–9344.
[9] K.G. Shyu, F.L. Hsu, M.J. Wang, B.W. Wang, S. Lin, Hypoxia-inducible factor 1alpha regulates lung adenocarcinoma cell invasion, Exp. Cell Res. 313 (2007) 1181–1191.
[10] M. Hockel, K. Schlenger, S. Hockel, B. Aral, U. Schaffer, P. Vaupel, Tumor hypoxia in pelvic recurrences of cervical cancer, Int. J. Cancer 79 (1998) 365–369.
[11] A.L. Harris, Hypoxia—a key regulatory factor in tumour growth, Nat. Rev. Cancer 2 (2002) 38–47.
[12] P. Carmeliet, R.K. Jain, Angiogenesis in cancer and other diseases, Nature 407 (2000) 249–257.
[13] D.R. Fels, C. Koumenis, The PERK/eIF2alpha/ATF4 module of the UPR in hypoxia resistance and tumor growth, Cancer Biol. Ther. 5 (2006) 723–728.
[14] P. Vaupel, L. Harrison, Tumor hypoxia: causative factors, compensatory mechanisms, and cellular response, Oncologist 9 (Suppl. 5) (2004) 4–9.
[15] R.A. Cardone, V. Casavola, S.J. Reshkin, The role of disturbed pH dynamics and the Na+/H+ exchanger in metastasis, Nat. Rev. Cancer 5 (2005) 786–795.
[16] K.M. Comerford, T.J. Wallace, J. Karhausen, N.A. Louis, M.C. Montalto, S.P. Colgan, Hypoxia-inducible factor-1-dependent regulation of the multidrug resistance (MDR1) gene, Cancer Res. 62 (2002) 3387–3394.
[17] J.P. Piret, D. Mottet, M. Raes, C. Michiels, $CoCl_2$, a chemical inducer of hypoxia-inducible factor-1, and hypoxia reduce apoptotic cell death in hepatoma cell line HepG2, Ann. N. Y. Acad. Sci. 973 (2002) 443–447.
[18] G.L. Semenza, Targeting HIF-1 for cancer therapy, Nat. Rev. Cancer 3 (2003) 721–732.
[19] G.L. Semenza, Evaluation of HIF-1 inhibitors as anticancer agents, Drug Discov. Today 12 (2007) 853–859.
[20] D.J. Manalo, A. Rowan, T. Lavoie, L. Natarajan, B.D. Kelly, S.Q. Ye, J.G. Garcia, G.L. Semenza, Transcriptional regulation of vascular endothelial cell responses to hypoxia by HIF-1, Blood 105 (2005) 659–669.
[21] J.P. Piret, J.P. Cosse, N. Ninane, M. Raes, C. Michiels, Hypoxia protects HepG2 cells against etoposide-induced apoptosis via a HIF-1-independent pathway, Exp. Cell Res. 312 (2006) 2908–2920.
[22] P. Gong, B. Hu, D. Stewart, M. Ellerbe, Y.G. Figueroa, V. Blank, B.S. Beckman, J. Alam, Cobalt induces heme oxygenase-1 expression by a hypoxia-inducible factor-independent mechanism in Chinese hamster ovary cells: regulation by Nrf2 and MafG transcription factors, J. Biol. Chem. 276 (2001) 27018–27025.
[23] A. Miyoshi, Y. Kitajima, T. Ide, K. Ohtaka, H. Nagasawa, Y. Uto, H. Hori, K. Miyazaki, Hypoxia accelerates cancer invasion of hepatoma cells by upregulating MMP expression in an HIF-1alpha-independent manner, Int. J. Oncol. 29 (2006) 1533–1539.
[24] T.D. Ardyanto, M. Osaki, N. Tokuyasu, Y. Nagahama, H. Ito, $CoCl_2$-induced HIF-1alpha expression correlates with proliferation and apoptosis in MKN-1 cells: a possible role for the PI3K/Akt pathway, Int. J. Oncol. 29 (2006) 549–555.
[25] P. Hook, R.B. Vallee, The dynein family at a glance, J. Cell. Sci. 119 (2006) 4369–4371.
[26] K.K. Pfister, E.M. Fisher, I.R. Gibbons, T.S. Hays, E.L. Holzbaur, J.R. McIntosh, M.E. Porter, T.A. Schroer, K.T. Vaughan, G.B. Witman, S.M. King, R.B. Vallee, Cytoplasmic dynein nomenclature, J. Cell Biol. 171 (2005) 411–413.
[27] K. Oiwa, H. Sakakibara, Recent progress in dynein structure and mechanism, Curr. Opin. Cell. Biol. 17 (2005) 98–103.
[28] J.R. Levy, E.L. Holzbaur, Cytoplasmic dynein/dynactin function and dysfunction in motor neurons, Int. J. Dev. Neurosci. 24 (2006) 103–111.
[29] K. Inaba, Molecular architecture of the sperm flagella: molecules for motility and signaling, Zool. Sci. 20 (2003) 1043–1056.
[30] M.W. Pfaffl, A new mathematical model for relative quantification in real-time RT-PCR, Nucleic Acids Res. 29 (2001) e45.
[31] T. Mosmann, Rapid colorimetric assay for cellular growth and survival: application to proliferation and cytotoxicity assays, J. Immunol. Methods 65 (1983) 55–63.
[32] J.X. Yan, A.T. Devenish, R. Wait, T. Stone, S. Lewis, S. Fowler, Fluorescence two-dimensional difference gel electrophoresis and mass spectrometry based proteomic analysis of *Escherichia coli*, Proteomics 2 (2002) 1682–1698.
[33] R. Sullivan, C.H. Graham, Hypoxia-driven selection of the metastatic phenotype, Cancer Metastasis Rev. 26 (2007) 319–331.
[34] T.G. Obrig, W.J. Culp, W.L. McKeehan, B. Hardesty, The mechanism by which cycloheximide and related glutarimide antibiotics inhibit peptide synthesis on reticulocyte ribosomes, J. Biol. Chem. 246 (1971) 174–181.
[35] D. Nandi, P. Tahiliani, A. Kumar, D. Chandu, The ubiquitin–proteasome system, J. Biosci. 31 (2006) 137–155.
[36] D.H. Lee, A.L. Goldberg, Proteasome inhibitors: valuable new tools for cell biologists, Trends Cell Biol. 8 (1998) 397–403.
[37] H. Zhong, A.M. De Marzo, E. Laughner, M. Lim, D.A. Hilton, D. Zagzag, P. Buechler, W.B. Isaacs, G.L. Semenza, J.W. Simons, Overexpression of hypoxia-inducible factor 1alpha in common human cancers and their metastases, Cancer Res. 59 (1999) 5830–5835.
[38] S.M. Larson, Positron emission tomography-based molecular imaging in human cancer: exploring the link between hypoxia and accelerated glucose metabolism, Clin. Cancer Res. 10 (2004) 2203–2204.
[39] W. Sun, J. Zhang, O. Hankinson, A mutation in the aryl hydrocarbon receptor (AHR) in a cultured mammalian cell line identifies a novel region of AHR that affects DNA binding, J. Biol. Chem. 272 (1997) 31845–31854.
[40] S. Wellmann, C. Buhrer, E. Moderegger, A. Zelmer, R. Kirschner, P. Koehne, J. Fujita, K. Seeger, Oxygen-regulated expression of the RNA-binding proteins RBM3 and CIRP by a HIF-1-independent mechanism, J. Cell. Sci. 117 (2004) 1785–1794.
[41] L. Xi, M. Taher, C. Yin, F. Salloum, R.C. Kukreja, Cobalt chloride induces delayed cardiac preconditioning in mice through selective activation of HIF-1alpha and AP-1 and iNOS signaling, Am. J. Physiol. Heart Circ. Physiol. 287 (2004) H2369–H2375.
[42] G. Fink, G. Steinberg, Dynein-dependent motility of microtubules and nucleation sites supports polarization of the tubulin array in the fungus *Ustilago maydis*, Mol. Biol. Cell. 17 (2006) 3242–3253.
[43] T. van den Beucken, M. Koritzinsky, B.G. Wouters, Translational control of gene expression during hypoxia, Cancer Biol. Ther. 5 (2006) 749–755.
[44] I. Stein, A. Itin, P. Einat, R. Skaliter, Z. Grossman, E. Keshet, Translation of vascular endothelial growth factor mRNA by internal ribosome entry: implications for translation under hypoxia, Mol. Cell. Biol. 18 (1998) 3112–3119.
[45] J. Fandrey, A. Huwiler, S. Frede, J. Pfeilschifter, W. Jelkmann, Distinct signaling pathways mediate phorbol-ester-induced and cytokine-induced inhibition of erythropoietin gene expression, Eur. J. Biochem. 226 (1994) 335–340.
[46] R. Rathore, Y.M. Zheng, C.F. Niu, Q.H. Liu, A. Korde, Y.S. Ho, Y.X. Wang, Hypoxia activates NADPH oxidase to increase [ROS]i and [Ca2+]i through the mitochondrial ROS-PKCepsilon signaling axis in pulmonary artery smooth muscle cells, Free Radic. Biol. Med. 45 (2008) 1223–1231.
[47] M.D. Short, S.M. Fox, C.F. Lam, K.R. Stenmark, M. Das, Protein kinase Czeta attenuates hypoxia-induced proliferation of fibroblasts by regulating MAP kinase phosphatase-1 expression, Mol. Biol. Cell 17 (2006) 1995–2008.
[48] J.W. Lee, J.A. Park, S.H. Kim, J.H. Seo, K.J. Lim, J.W. Jeong, C.H. Jeong, K.H. Chun, S.K. Lee, Y.G. Kwon, K.W. Kim, Protein kinase C-delta regulates the stability of hypoxia-inducible factor-1 alpha under hypoxia, Cancer Sci. 98 (2007) 1476–1481.
[49] Z. Lu, D. Liu, A. Hornia, W. Devonish, M. Pagano, D.A. Foster, Activation of protein kinase C triggers its ubiquitination and degradation, Mol. Cell. Biol. 18 (1998) 839–845.
[50] E.R. Griffis, N. Stuurman, R.D. Vale, Spindly, a novel protein essential for silencing the spindle assembly checkpoint, recruits dynein to the kinetochore, J. Cell Biol. 177 (2007) 1005–1015.
[51] K.W. Lo, H.M. Kan, K.K. Pfister, Identification of a novel region of the cytoplasmic Dynein intermediate chain important for dimerization in the absence of the light chains, J. Biol. Chem. 281 (2006) 9552–9559.
[52] P.S. Vaughan, J.D. Leszyk, K.T. Vaughan, Cytoplasmic dynein intermediate chain phosphorylation regulates binding to dynactin, J. Biol. Chem. 276 (2001) 26171–26179.